scientific reports

Check for updates

OPEN

Identifying ADME-related gene signature for immune landscape and prognosis in KIRC by single-cell and spatial transcriptome analysis

Hongyun Wang[1,2,6], Feizhou Li[1,6], Qiong Wang[2], Xinyuan Guo[2], Xinbing Chen[2], Xinrong Zou[1,2,3,4]✉ & Jun Yuan[5]✉

Kidney renal clear cell carcinoma (KIRC) is the most prevalent subtype of kidney cancer. Although multiple therapeutic agents have been proven effective in KIRC, their clinical application has been hindered by a lack of reliable biomarkers. This study focused on the prognostic value and function of drug absorption, distribution, metabolism, and excretion- (ADME-) related genes (ARGs) in KIRC to enhance personalized therapy. The critical role of ARGs in KIRC microenvironment was confirmed by single cell RNA-seq analysis and spatial transcriptome sequencing analysis for the first time. Then, an ADME-related prognostic signature (ARPS) was developed by the bulk RNA-seq analysis. The ARPS, created through Cox regression, LASSO, and stepAIC analyses, identified eight ARGs that stratified patients into high-risk and low-risk groups. High-risk patients had significantly poorer overall survival. Multivariate analysis confirmed the independent predictive ability of ARPS, and an ARPS-based nomogram was constructed for clinical application. Gene ontology and KEGG pathway analyses revealed immune-related functions and pathways enriched in these groups, with low-risk patients showing better responses to immunotherapy. Finally, the expression of ARGs was validated by qRT-PCR and Western blotting experiments. These findings underscore the prognostic significance of ARPS in KIRC and its potential application in guiding personalized treatment strategies.

Keywords Kidney renal clear cell carcinoma, ADME genes, Gene signature, Survival, Immune cell infiltration

Abbreviations

ADME	Absorption, distribution, metabolism, and excretion
ARGs	ADME-related genes
ARPS	ADME-related prognostic signature
ARS	ADME-related score
BP	Biological process
CNV	Copy number variation
CY	Cytochrome
DCA	Decision curve analysis
DEARGs	Differentially expressed ARGs
DEGs	Differentially expressed genes
DFS	Disease-free survival
ESCC	Esophageal squamous cell carcinoma
FBS	Fetal bovine serum
FC	Fold change

[1]Hubei Provincial Hospital of Traditional Chinese Medicine, Affiliated Hospital of Hubei University of Chinese Medicine, Wuhan 430061, China. [2]Hubei University of Chinese Medicine, Wuhan 430065, China. [3]Institute of Chinese Medicine Nephrology, Hubei Province Academy of Traditional Chinese Medicine, Wuhan 430074, China. [4]Hubei Key Laboratory of Theory and Application Research of Liver and Kidney in Traditional Chinese Medicine (Hubei Province Hospital of Traditional Chinese Medicine), Wuhan 430061, China. [5]Department of Nephrology, Renmin Hospital of Wuhan University, Wuhan 430060, China. [6] These authors contributed equally: Hongyun Wang and Feizhou Li. ✉email: zouxinrong@hbhtcm.com; yjun_92@hbucm.edu.cn

FDR	False discovery rate
GDSC	Genomics of drug sensitivity in cancer
GO	Gene ontology
HNSCC	Head and neck squamous cell carcinoma
HR	High-risk
IC50	Half maximal inhibitory concentration
ICGs	Immune checkpoint genes
ICI	Immune cell infiltration
KEGG	Kyoto Encyclopedia of Genes and Genomes
KIRC	Kidney renal clear cell carcinoma
KM	Kaplan-Meier
LASSO	The least absolute shrinkage and selection operator
LR	Low-risk
ME	Microenvironment
OS	Overall survival
PK	Pharmacokinetics
PPI	Protein-protein interaction
qRT-PCR	Quantitative real-time PCR
RCC	Renal cell carcinoma
ROC	Receiver operating characteristic
ssGSEA	Single-sample GSEA
TCGA	The Cancer Genome Atlas
TIDE	Tumor immune dysfunction and exclusion
TMB	Tumor mutation burden
TME	Tumor microenvironment
WB	Western Blotting

Kidney cancer, second only to bladder cancer with respect to incidence, represents one of the most prevalent cancer in genitourinary system, as revealed by epidemiological studies[1]. It is estimated that 90–95% of kidney cancers fall into the category of RCC, which mostly derive from the renal tubular epithelium[2]. KIRC represents the most prevalent histologic variant of RCC, accounting for over 75% of all renal tumors[3]. The incidence of RCC is on an upward trend[4]. KIRC patients' survival rate can be significantly improved via early detection and intervention[5]. Patients with stage I metastatic diseases have a 5-year relative survival rate of 93%, whereas it drops to 72.5% for those with stage II/III diseases and dramatically decreases to 12% for stage IV diseases[6]. Despite advances in treatment and early detection, about 30% of these patients are already in the metastatic stage at diagnosis[6], and approximately $20-50\%$ of patients with localized KIRC still face the daunting prospect of recurrence or metastasis following surgical tumor resection[1]. Thus, it is essential to determine novel prognostic and diagnostic markers in order to enhance the clinical management of this disease.

ADME-related genes (ARGs) are the genes linked to drug absorption, distribution, metabolism, and elimination processes, which have a pivotal role in pharmacokinetics[7]. The PharmaADME consortium has revealed that ARGs encompass 266 extended genes and 32 core genes (http://www.pharmaadme.org), including phase I and II drug-metabolizing enzymes, modifiers, and transporters that affect drug clearance and metabolism by the liver[8]. ARGs are extensively utilized in cancer research to understand their expression profiles in different cancer types and their impact on patient outcomes. Researchers have identified differential expression of ARGs in tumors, with some genes related to favorable overall survival (OS) rates in certain cancers, while others linked to unfavorable outcomes[9]. Studies have shown that ARGs may affect the survival of cancer patients through various mechanisms related to drug metabolism and disposition[10]. Tang et al. developed a novel ADME-related 14-gene prognosis model in HNSCC, the model assigned patients into two groups, i.e., the LR group or the HR group, and the results revealed that LR patients have significantly improved overall survival and disease free survival and benefit more from immunotherapy and chemotherapy[11]. In addition, ARGs are being explored as possible therapeutic targets and prognostic biomarkers in cancer treatment, highlighting their importance in personalized medication and patient management improvement[12]. Wang et al. established a risk score signature based on ARGs that distinguishes HR from LR sarcoma patients, demonstrating longer survival in the LR group and also offering a direction for future targeted therapies[13]. However, the biological roles and predictive value of ARGs in KIRC are still poorly understood.

In this study, We used single-cell sequencing and spatial transcriptome analysis for the first time, demonstrating the critical role of ARGs in the KIRC microenvironment (Fig. 1), followed by the analysis of bulk RNA-seq analysis. An 8-gene signature was defined for survival outcome prediction in TCGA training cohort via analyses of LASSO and stepAIC, and this method was verified using an external independent cohort. Then, analyses of functional enrichment, immune cell infiltration (ICI), drug sensitivity, and mutation were performed between the HR and LR groups. Finally, the PCR and Western experiment was conducted to validate the expression of the target genes. The results not only aim to improve the understanding of the genetic landscape of KIRC, but also to explore the impact of ARGs variations on patients' prognosis, thereby contributing to the personalized management of KIRC.

Materials and methods
Preprocessing and dataset source
In this study, the training cohort consisted of currently accessible treatment and expression data of KIRC patients obtained from TCGA (610 samples)(https://portal.gdc.cancer.gov/)[14]. The "TCGAbiolinks" package[15](version
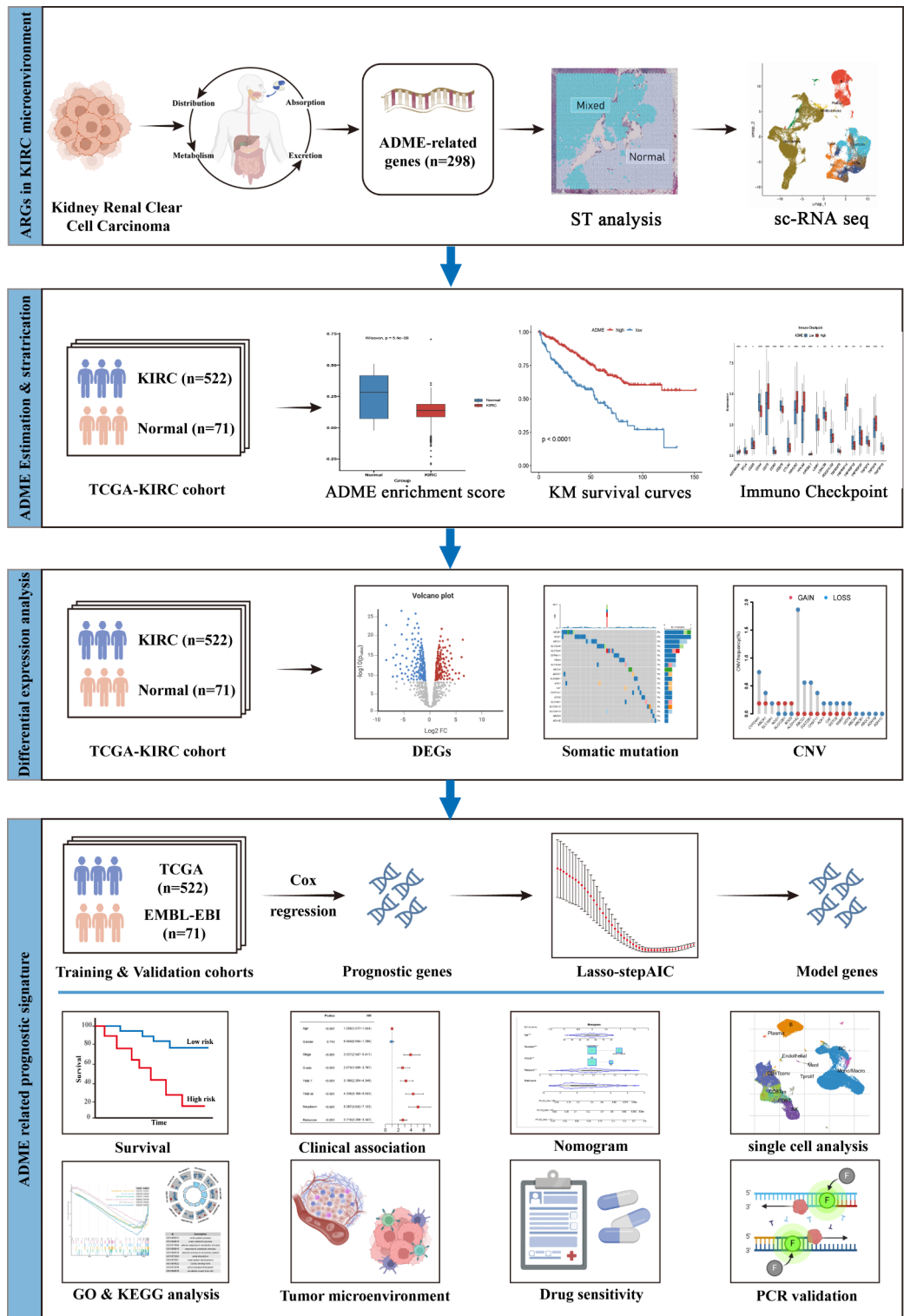
Fig. 1. Flowchart for comprehensive analysis of ADME-related gene signature for immune landscape and prognosis in patients with Kidney renal clear cell carcinoma (KIRC).

2.32.0) in R was employed to download RNA-seq data, the mutation profiles, and relevant clinical information. Additionally, information from EMBL-EBI database (https://www.ebi.ac.uk/) had been utilized to obtain an independent validation cohort, i.e., the E-MTAB-1980 cohort (101 samples)[16], . The human KIRC scRNA-seq dataset GSE139555 (32 samples) was obtained from TISCH (http://tisch.comp-genomics.org/)[17]. KIRC spatial transcriptome dataset GSE175540 (24 samples) was obtained from Gene Expression Omnibus (https://www.ncb

i.nlm.nih.gov/geo/). A group of ARGs ($n = 298$) was derived from PharmaADME consortium (http://www.pharmaadme.org)[7]. Regarding the handling of missing values, we remove the missing values directly.

Processing KIRC spatial transcriptome sequencing data

Spatial transcriptome data analysis was conducted using the R package Seurat[18](version 5.1.0). This involved normalizing unique molecular identifier (UMI) counts, scaling the data, and identifying the most variable features using "SCTransform"[19]. Subsequently, downscaling and unsupervised cluster analysis were performed using "RunPCA". For cluster analysis, default parameters were utilized, focusing on the 30 most significant principal components. Additionally, the "SpatialFeaturePlot" function was employed for subgroup and gene visualization. The "AUCell" R package[20] (version 1.26.0) serves as a valuable tool for spatial transcriptome ADME related gene analysis. Its primary function is to quantify and visualize ADME related activities at spatial transcriptome resolution.

scRNA-seq data analysis

The 10× scRNA-seq data GSE139555 were converted to Seurat object using "Seurat" R package. The clusters with cells < 3, cells with < 50 genes, and cells with > 5% of mitochondrial genes were removed. Principal component analysis (PCA) was performed using the top 1500 most variable genes. The "FindNeighbors" and "FindClusters" functions were applied for cell clustering analysis based on the top 15 principal components (PCs). The "FindAllMarkers" function was utilized to identify marker genes in different cell clusters, with FDR < 0.01 and |log2FC| > 1 as the threshold. Furthermore, clusters were annotated to recognize different cell types using "CellMarker 2.0" database[21]. The "ssGSEA" function in the Seurat package was utilized to quantify the activity of a specific gene set in each cell.

Calculation of ARS and definition of optimal cutoff

The GSVA package (version 1.52.3) was selected to conduct ssGSEA analysis so as to obtain the ARS. The "surv_cutpoint" in the R package "survminer"[10] (version 0.4.9) was employed to determine optimal ARS and cutoff for statistical analysis.

Identification of DEARGs and functional analysis

For KIRC cases and normal cases in TCGA datasets, DEARGs were discovered using the R package "limma"[22] (version 3.60.3). Notably, the cutoff was defined as FDR < 0.05 and log2|FC| > 1. ARGs were characterized by both KEGG pathway[23–25] and GO pathway, which was identified using the clusterProfiler package[26] (version 4.12.6) in R to investigate their potential biological roles and signaling pathways. In case of FDR < 0.1, the result was determined to have statistical significance.

Identification of ADME-related subtypes

R package "ConsensusClusterPlus" (version 1.68.0) was utilized to identify ADME-related molecular clusters. Furthermore, the correlations of ADME-related clusters with clinicopathologic characteristics and survival of KIRC patients was explored. Respectively, using ESTIMATE method and CIBERSORT algorithm, the dissimilarity of immune microenvironment and immune infiltrating cells among different ADME-related molecular clusters were particularly revealed. Gene Set Variation Analysis (GSVA) was used to investigate the potential mechanism between ADME-related molecular clusters, with a significance threshold of value of FDR < 0.05.

Construction and validation of ARPS

The stepAIC analysis using MASS package (version 7.3–61) and the LASSO analysis using the glmnet package (version 4.1-8) were then performed to identify the most predictive ARGs for KIRC prognosis in line with DEARGs. We used the LASSO-Cox regression model to screen for the best prognostic biomarkers, determined lambda values by ten-fold cross-validation, and multivariate cox analyses to obtain regression coefficients for each gene and construct Cox regression risk scores. All patients were assigned into the LR and HR groups according to the median risk scores. In addition, analyses of time-dependent ROC and KM were implemented to evaluate the prognostic performance of ARPS. An external independent validation cohort used data from E-MTAB-1980 to determine the generalization degree of ARPS. Ultimately, the prognostic independence was estimated for clinical parameters such as ADME-related risk scores in KIRC patients via analyses of univariate and multivariate Cox regression. In order to create a nomogram that would predict the survival, important risk variables were incorporated. Calibration curves were plotted and a DCA was implemented to assess the nomogram's precision.

Immunogenomic landscape assessment

Using marker genes for immune cells of 28 types[27] as a reference gene set, the abundance was estimated for immune cells in each patient using the ssGSEA. In addition, the relative proportions for immune cells of 22 types were estimated via the CIBERSORT R package[28](version 0.1.0). The R package "estimate" (version 1.0.13) was then chosen to compute the score of ESTIMATE, stroma, and immunity so as to evaluate the tumor purity. The tumor immune dysfunction and exclusion (TIDE) score was calculated using the online server (http://tide.dfci.harvard.edu)[29] so as to evaluate possible clinical effect of immunotherapy in various risk groups. The hypoxia score of KIRC was acquired from cBioPortal (https://www.cbioportal.org/)[30].

Prediction of drug response to ARPS

Using pharmacogenomic information from the GDSC database, this study predicted drug sensitivity for the enrolled cases of KIRC. Using the pRRophetic package[31](version 0.5), IC50 was calculated to reflect the drug response.

Stemness signatures analysis

First, StemChecker (http://stemchecker.sysbiolab.eu/)[32] was used for the recruitment of 26 stemness gene sets in this study. The most extensive and most recent compilation of published stemness signatures, which were determined by computational summaries, literature transcription factor target gene sets, RNAi screens, and gene expression profiles, served as the foundation for this tool. Then, using the GSVA R package, the stemness enrichment scores were calculated for the 26 stemness gene sets in each KIRC sample via ssGSEA and the analysis of differential gene expression was performed in both groups.

Cell incubation

The human kidney cell lines, including Caki-1, 786-O, and HK-2, were purchased from Wuhan Pricella Biotechnology Co., Ltd. The 10% FBS-enriched minimum essential medium was utilized to sustain HK-2 cells. The 10% FBS-enriched RPMI-1640 medium was used to sustain 786-O cells. Caki-1 cells were also sustained in 10% FBS-enriched McCoy's 5 A medium. Each cell line was cultured in a 37 °C humidified environment with 5% CO2. All cell lines underwent authentication via short tandem repeat DNA profiling and were confirmed to have no contamination of mycoplasma.

qRT-PCR and RNA extraction

Samples were subjected to total RNA extraction using the TRIzol reagent (Vazyme, China) based on the manufacturer's instructions. The A260/A280 ratio was measured to assess the concentration of RNA using NanoDrop. The PrimeScript RT Reagent Kit (TransGen Biotech, China, AT341-02) was utilized for cDNA synthesis, and the SYBR Green PCR Reagent (ChamQ Universal, China, Q711-02) was adopted for qRT-PCR based on the protocol of the manufacturer. The reaction consisted of a 3-minute initial incubation and 40 cycles of 15-second denaturation, both at 95 °C, as well as 1-minute annealing/extension at 60 °C. The internal control was implemented with β-Actin. In Supplementary Table 1, primer sequences are provided. For data analysis for relative quantification, the $2^{-\Delta\Delta CT}$ method was employed.

Western blot assay

Proteins were isolated from Caki-1, 786-O, and HK-2 cell lines using RIPA buffer. A BCA protein assay kit was employed for quantifying protein concentrations. After electrophoresis on a 10% SDS-PAGE gel, the proteins were transferred to a PVDF membrane, which was blocked for an hour at room temperature using 5% BSA. Then, it was cultured overnight at 4 °C using primary antibodies against ABCB1, ALDH5A1, and β-actin (Proteintech Group, Inc.; dilutions of 1:500, 1:1000, and 1:5000, respectively). Secondary antibodies were applied at 1:5000 and cultured at room temperature for one hour. ImageJ software was employed to quantify relative protein expression levels.

Statistical analysis

This study applied R software (v4.3.1) for all statistical analyses. A pairwise comparison between the two groups was performed by the Wilcoxon test, and a multiple group comparison was implemented by the Kruskal-Wallis test (*$p < 0.05$; **$p < 0.01$; ***$p < 0.001$; ****$p < 0.0001$). The log-rank test and the KM method were used for the survival analysis. In case of $p < 0.05$, the result was determined to have statistical significance.

Results

ADME-related characteristic in spatial transcriptome and scRNA-seq

We employed SCTransform's approach to correct for spatial sequencing depth and conducted a series of normalization processes, resulting in the identification of 12 distinct cell types in space following dimensionality reduction clustering (Figure S1). To evaluate the importance of ADME related genes in each cell subset, we used the AUCell R package to determine the ADME related activity in each cell subgroup (Fig. 2A). We found that ADME related activity was predominantly enriched in tumor cells (Fig. 2B-C). Subsequently, we used spearman correlation analysis to calculate the correlation between cell content and cell content, as well as the correlation between cell content and ADME related activity in all spots (Fig. 2D). scRNA-seq data, comprising 49,899 cells, were obtained from three early KIRC patients. Using marker genes for different cell types, we annotated the cells into 11 major clusters, including B cell, CD4Tconv, CD8T, CD8Tex, dendritic cell, endothelial cell, mast cell, monocyte/macrophage, NK cell, Plasma cell, and Tprolif cell (Fig. 2E). To quantify the activity of the ADME in different cell types, we used the "ssGSEA" function in the Seurat package to calculate the expression levels of ADME-related genes across all cells (Fig. 2F). Of the 11 cell types, ADME related activity was notably higher in endothelial cell and monocyte/macrophage (Fig. 2G).

ARS estimation and stratification analysis in KIRC patients

The ARS was calculated using the ssGSEA algorithm for 522 patients with KIRC and 71 normal patients derived from the TCGA database. Compared to the control group, a significantly lower ARS was observed in the KIRC group, which evidenced the accuracy of the model (Fig. 3A). Then, the association between ARS and clinical parameters in KIRC patients were further investigated. A higher ARS was associated with a lower stage, T and M (Fig. 3B-D). The optimal cutoff for ARS was determined to be 0.1 using the "surv_cutpoint" function (Fig. 3E). Based on this cutoff, KIRC patients were arranged to two groups (high-ARS group and low-ARS
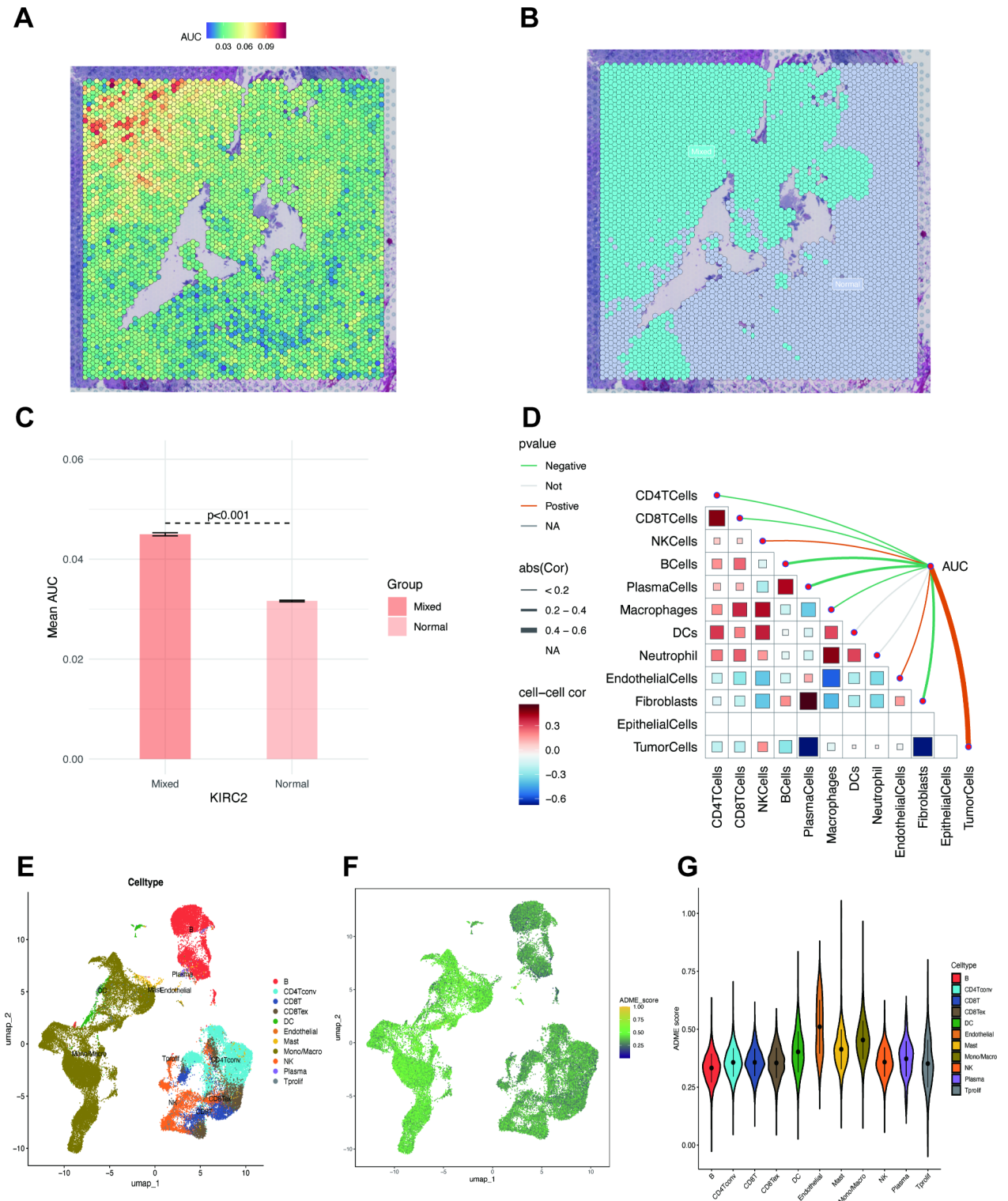
Fig. 2. ADME-related characteristic in spatial transcriptome and scRNA-seq. (**A**) Spatial visualization of ADME intensity. (**B-C**) Differential anlysis of ADME related activity in mixed malignant, and normal regions. (**D**) Spearman correlation of ADME related activity with microenvironmental components at spatial transcriptome resolution. (**E**) Single cell types identified by marker genes. (**F**) The ADME enrichment score (activity) in each cell. (**G**) The distribution of ADME score in different cell types. *$p < 0.05$; **$p < 0.01$; ***$p < 0.001$; ****$p < 0.0001$. ADME: Absorption, distribution, metabolism and excretion.
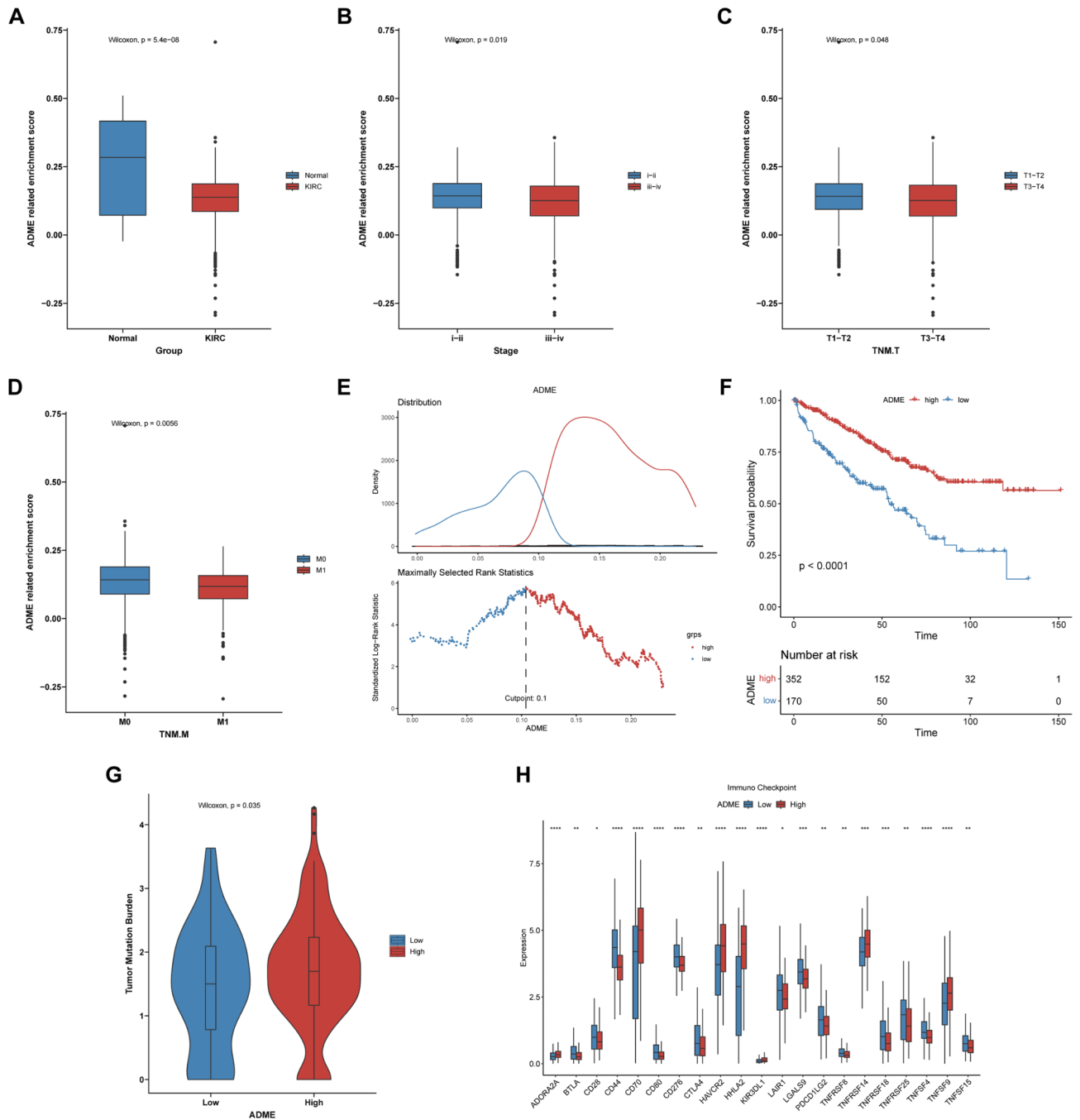
Fig. 3. ARS estimation and stratification analysis in KIRC patients. (**A**) Box plot showing the differences in ssGSEA ARS between KIRC and normal samples by Wilcoxon test. Box plot comparing ssGSEA ARS between (**B**) Stage, (**C**) TNM.T, (**D**) TNM.M., (**E**) KIRC patients were divided into the low-ARS and high-ARS groups using the surv_cutpoint function. (**F**) KM survival curves of the OS for KIRC patients in the high-ARS and low-ARS groups. (**G**) Comparison of TMB between the high-ARS and low-ARS groups. (**H**) Comparison of the immune checkpoint between the high-ARS and low-ARS groups. *$p < 0.05$; **$p < 0.01$; ***$p < 0.001$; ****$p < 0.0001$. TMB: Tumor mutation burden. ADME: Absorption, distribution, metabolism and excretion.

group). Compared to the low-ARS group, the high-ARS group had a better OS (Fig. 3F). In addition, this study computed tumor mutation burden (TMB) for each KIRC patient. As predicted, the low-ARS group generally had lower TMB than the high-ARS group (Fig. 3G). Given the pivotal role that immune checkpoint inhibitors play in clinical treatment of KIRC, the differential expression of ICGs was analyzed, and the results revealed that CD28, CD44, CD88, PDCD1LG2, and CD276 increased significantly in the LR group, whereas CD70, HHLA2, TNFRSF14, and TNFSF9 increased in the HR group (Fig. 3H).

Variant landscape of ARGs in KIRC patients

This study screened 58 DEGs for KIRC and normal groups to investigate the distinct transcriptomic signatures (Fig. 4A-B). Subsequently, the intricate relevance of DEG-associated proteins was clarified by constructing a network of interactions between proteins (Fig. 4C). Additionally, the molecular alteration landscape of ADME-related DEGs in KIRC was examined, and the most prevalent type of variant was the missense mutation (Fig. 4D). ABCB1, NOS1, ABCA1, SLC22A6, and SLC15A2 are the top five mutated genes. The top 20 mutated ADME-related DEGs exhibited significant CNV alterations, based on the investigation of CNV mutation frequency (Fig. 4E). R software was employed for analyses of GO and KEGG enrichment so as to examine the regulatory
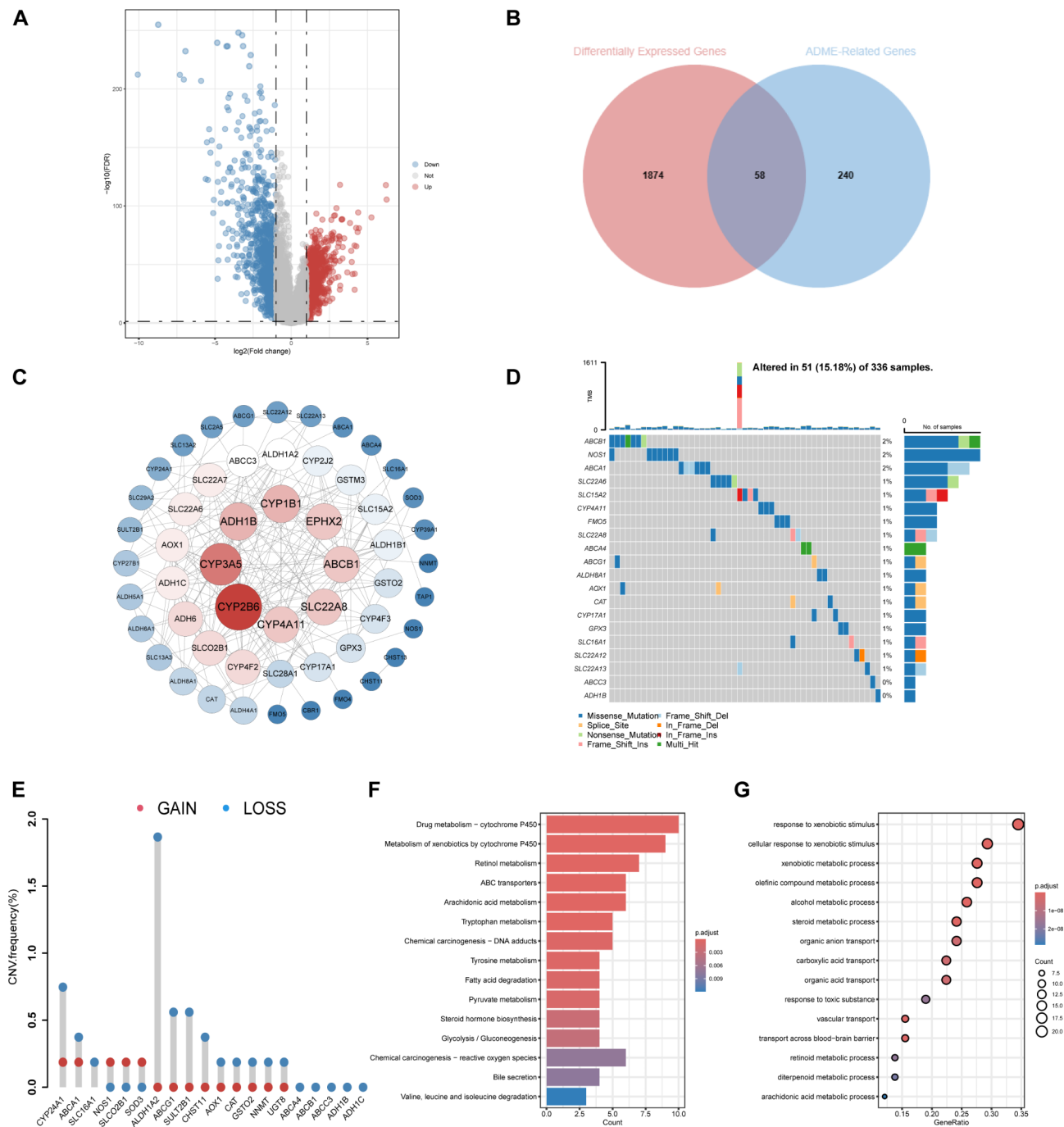
Fig. 4. Variant landscape of ARGs in KIRC patients. (**A**) Volcano plot of DEGs in KIRC (blue: downregulated DEGs; red: upregulated DEGs; gray: unchanged genes), FDR < 0.05 and |log2FC| > 1. (**B**) Venn diagram between KIRC DEGs and ARGs. (**C**) PPI network of ADME-related DEGs. (**D**) Oncoplot of the top 20 ADME-related DEGs in the TCGA cohort. (**E**) Frequencies of CNV gain, loss, and non-CNV among the top 20 ADME-related DEGs. (**F**) Bar plot of KEGG analysis of ADME-related in KIRC. (**G**) Dot plot of GO BP analysis of ADME-related in KIRC. GO, Gene ontology; KEGG, Kyoto Encyclopedia of Genes and Genomes.

mechanism of DEGS. According to the KEGG enrichment analysis, most of the enriched pathways contained drug metabolism-CYP450, ABC transporters, xenobiotic metabolism by CYP450, arachidonic acid metabolism, and retinol metabolism (Fig. 4F). Most of these genes were found to be enriched in response to xenobiotic metabolism, cellular response to xenobiotic stimulus, olefinic compound metabolism, xenobiotic stimulus, and steroid metabolism in the biological process(BP) analysis (Fig. 4G).

Subtype identification, TME infiltration characteristics, and biological signal features of two distinct ADME related clusters in KIRC

Then, we performed the unsupervised clustering analysis of the expression of 58 ADME related DEGs in 522 samples to explore the classification of KIRC by increasing the clustering matrix (k) from 2 to 10. As a result, consensus clustering was most suitable when k = 2, and three molecular subtypes were identified and named Cluster A-B (Fig. 5A-B). Cluster A contained 270 cases and Cluster B contained 252 cases. The relationship between the molecular subtypes and the clinical features, including the Grade, Stage, T, M, gender, survival status, and age was shown in the heatmap (Fig. 5C, E). Additionally, the two ADME molecular subtypes have different prognoses, as seen by the K-M curves, with the A cluster having a clear prognostic advantage ($p < 0.0001$, Fig. 5D). Furthermore, Cluster B displayed more immune cell infiltration than Cluster A (Fig. 5F). In particular, there was a significant increase in the immune infiltration level of T cells CD8, T cells regulatory Tregs, monocytes and Mast cells resting in Cluster A patients, while that of plasma cells and M1 macrophages increased in Cluster B patients (Fig. 5G). To explore potential differences in biological functions between ADME molecular subtypes, we performed Gene Set Variation Analysis (GSVA), several biology processes with differential expression were enriched, and they were shown in a heatmap. Compared with Cluster B, aldehyde catabolic process, xenobiotic export from cell, butanoate metabolism, fatty acid metabolism, citrate cycle (TCA cycle) were higher in Cluster A, while presynaptic cytoskeleton, collagen fibril organization, fibrillar collagen trimer and extracellular matrix structural constituent were higher in Cluster B (Fig. 5E). These findings suggest that ADME plays a crucial role in shaping the TME and that the two molecular subtypes exhibit distinct prognoses and molecular functions.

Construction of ARPS in KIRC

Univariate Cox regression analysis was conducted to screen ARGs with prognostic value so as to construct a prognostic gene model. As a result, 32 genes were found to have a significant prognostic value ($p < 0.05$). Analyses of LASSO and stepAIC were conducted to screen the target genes and simplify the model, producing an ultimate collection of 8 ARGs with coefficients to construct the prognosis model (Fig. 6A-C). The 8-gene prognosis model was defined in the following way: risk score = (-0.1467) * ABCB1 + (-0.2649) * ABCG1 + (0.3684) * ALDH5A1 + (-0.4660) * ALDH6A1 + (-0.1063) * DPEP1 + (-0.1780) * GSTM3 + (-0.1186) * SLC28A1 + (-0.2180) * UGT8. Patients with KIRC were stratified into the HR ($n = 261$) and the LR groups ($n = 261$) according to the median of signature. It was noteworthy that in the TCGA cohort, the LR group outperformed the HR group in terms of OS rate (median time = 47.0 months vs. 34.5 months, $p < 0.0001$, Fig. 6D). The independent validation cohort, E-MTAB-1980 cohort, was utilized to confirm the model's robustness, and the results demonstrated that the LR group also outperformed the HR group in terms of OS (median time = 53.0 months vs. 49.5 months, $P = 0.0098$, Fig. 6G). Additionally, AUC was evaluated for E-MTAB-1980 and TCGA cohorts, respectively, and the results indicated that ARPS had a high degree of accuracy in forecasting the 1-, 3-, and 5-year survival in KIRC patients (Fig. 6E & H). The distribution of survival status and risk scores is presented in Fig. 6F & I for TCGA and E-MTAB-1980 cohorts, separately. These findings confirm the strong performance of ADME-related prognosis model for predicting KIRC patients' outcome across various datasets.

Construction and assessment of nomogram

To assess the effect of ADME-related signatures in prognosis prediction, researchers in this study implemented univariate and multivariate Cox regression analyses. According to the results of univariate Cox regression analysis, age, T, stage, M, grade, neoplasm status, and risk score had a significant association with OS. According to the multivariate Cox regression analysis, M, age, risk score, and neoplasm status had an association with OS in KIRC patients (HR = 1.026, 95% CI [1.010–1.042], $p < 0.001$; HR = 1.767, 95% CI [1.142–2.732], $p = 0.010$; HR = 2.562, 95% CI [1.693–3.877], $p < 0.001$; HR = 1.974, 95% CI [1.524–2.558], $p < 0.001$) (Fig. 7A-B). This study also created a nomogram for the 1-, 3-, and 5-year survival prediction in KIRC patients based on the above correlation between clinicopathologic features and ADME-related signature (Fig. 7C). Using the same nomogram, the risk score was computed for all patients, and the patients were assigned in line with their risk scores. The prognosis for the LR and HR groups differs significantly (median time = 50.0 months vs. 35.4 months, $P < 0.001$, Fig. 7D). Additionally, the combined model has AUCs for the 1-, 3-, and 5-year survival of 0.831, 0.825, and 0.806, respectively (Fig. 7E). Moreover, the nomogram's predictive accuracy was shown via the calibration curve (Fig. 7F). Furthermore, a DCA (Fig. 7G) was carried out to compare the nomogram's clinical applicability with regard to the 1-, 3-, and 5-year survival. The results demonstrated that the 3- and 5-year OS was better predicted by the nomogram, which provided more net clinical benefit than the 1-year OS. In general, when utilizing these essential clinical parameters to assess KIRC patients' prognosis, the nomogram demonstrated solid prediction power and clinical applicability.

Immune characteristics of ADME-related prognostic subgroups

The TCGA KIRC cohort was employed to examine the association between ARPS and patients' immune status. In addition to interfering with tumor signaling, the vast majority of normal cells found in tumor tissue are infiltrating immune and stromal cells that regulate cancer biology. Using ESTIMATE algorithm, the immune ME landscape was investigated so as to understand the correlation between the ADME-related risk score signature and the biological role in immune response better. This algorithm demonstrated that a high immune
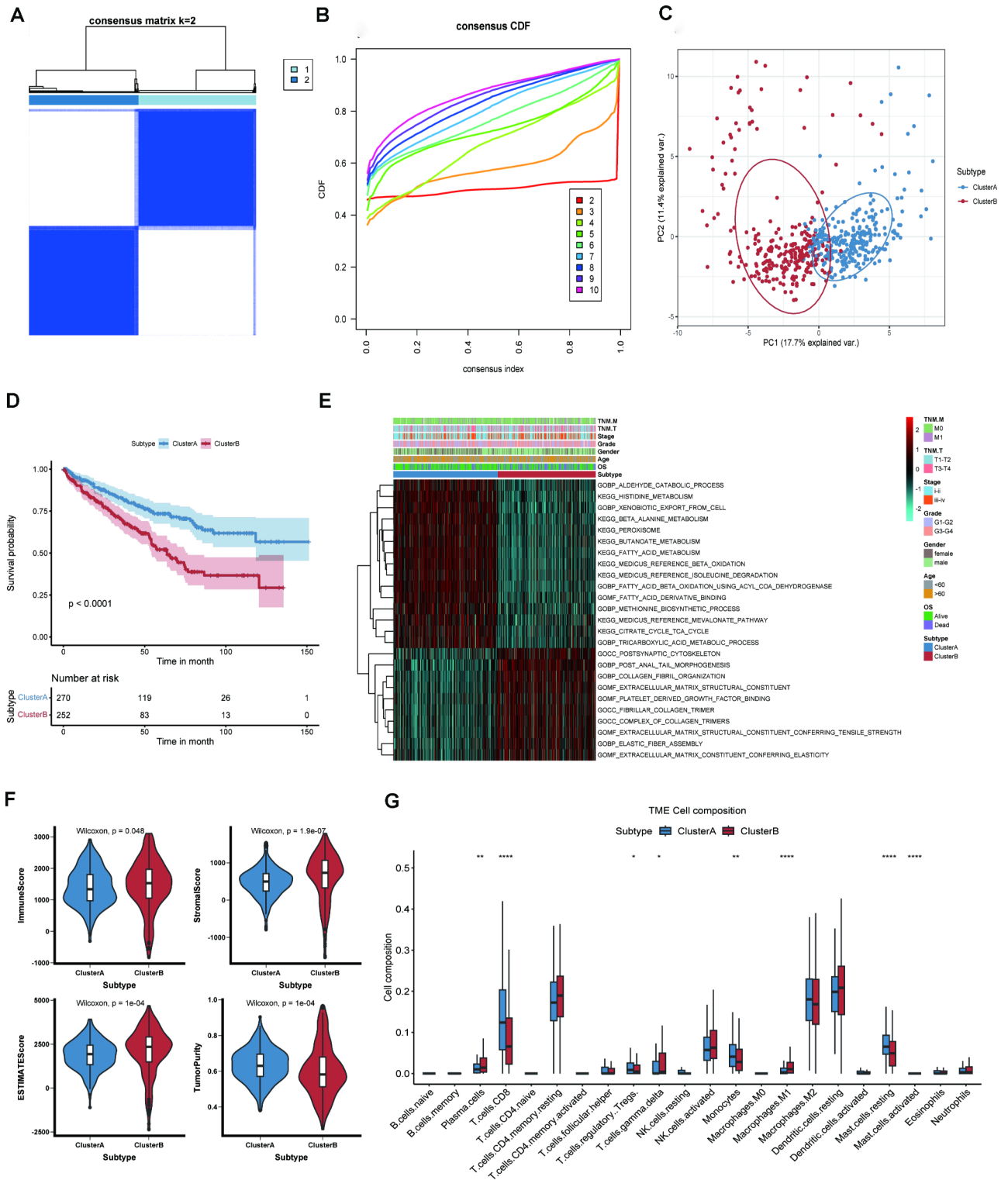
Fig. 5. Subtype identification, TME infiltration characteristics, and biological signal features of two distinct ADME related clusters in KIRC. (**A**). Samples from the TCGA-KIRC cohort were divided into two clusters using a consensus clustering algorithm (k = 2). (**B**) Cumulative Distribution Function (CDF) from k = 2 to 10. (**C**) Principal Component Analysis (PCA) shows significant differences between the two ADME clusters. (**D**) Kaplan-Meier curve shows different overall survival (OS) between the two ADME clusters. (**E**) Heatmap shows differences in clinical characteristics and biological functions between two ADME clusters. (**F**) The violin plot shows higher immune infiltration, stromal, and ESTIMATE score and lower TumorPurity in ClusterB. (**G**) The boxplot of 28 infiltrated immune cell types was calculated by CIBERSORT between the two ADME clusters. $*p < 0.05$; $**p < 0.01$; $***p < 0.001$; $****p < 0.0001$.
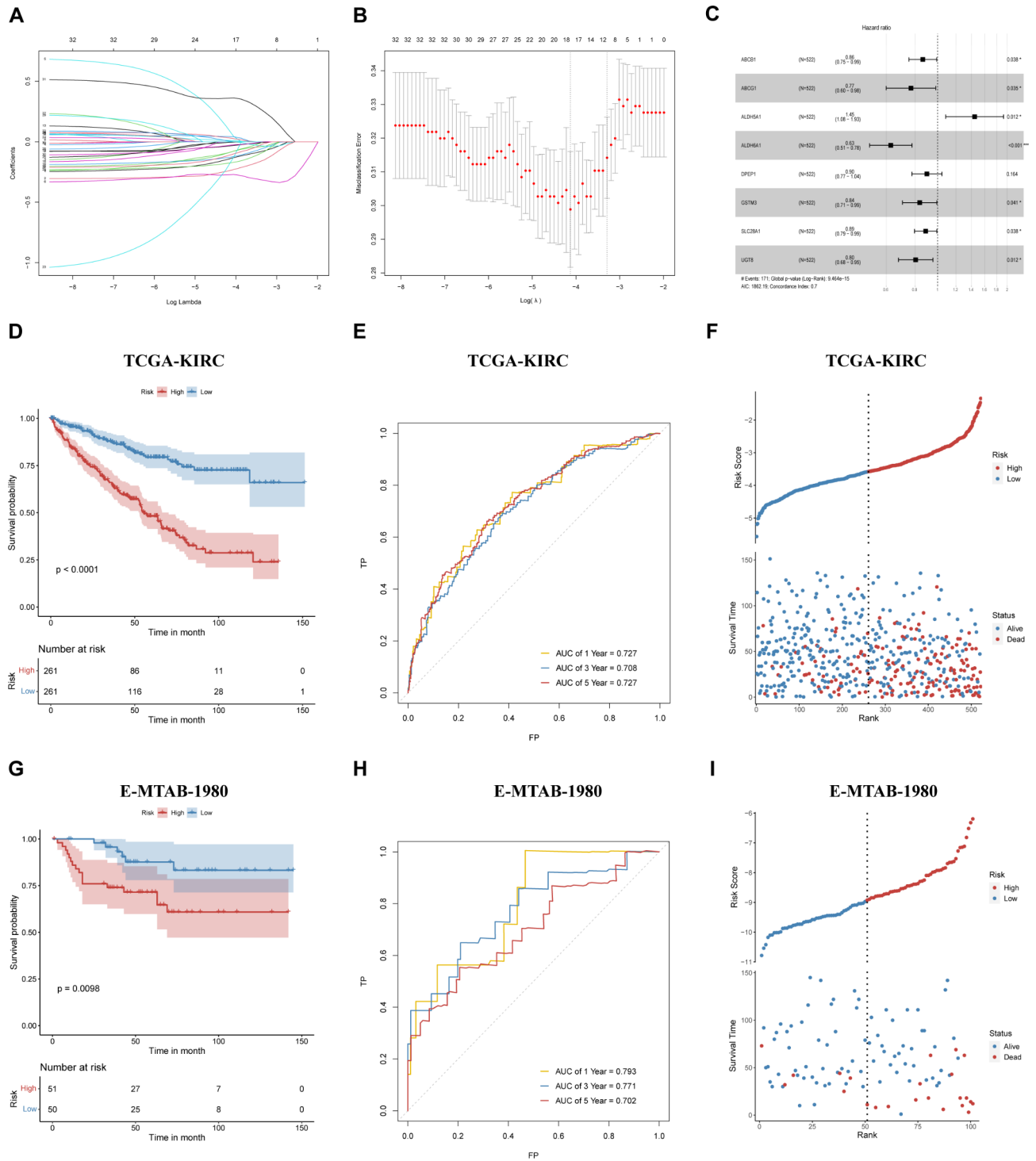
Fig. 6. Construction of an ARPS for KIRC patients. (A-B). LASSO regression analysis of ADME-related DEGs. The coefficients changed with increasing lambda value. (**C**) Forest plot of the final eight prognostic genes in the risk model from the stepAIC regression analysis. (**D**) OS of patients in the LR and HR score groups in TCGA-KIRC. (**E**) ROC curve of the risk model in predicting survival in TCGA-KIRC. (**F**) Distribution of risk score by the survival status and time in TCGA-KIRC. (**G**) OS of patients in the LR and HR score group in E-MTAB-1980. (**H**) ROC curve of the risk model in predicting survival in E-MTAB-1980. (**I**) Distribution of risk score by the survival status and time in E-MTAB-1980. LASSO: Least absolute shrinkage and selection operator; stepAIC: Stepwise Akaike information criterion; ROC: Receiver operator characteristic.
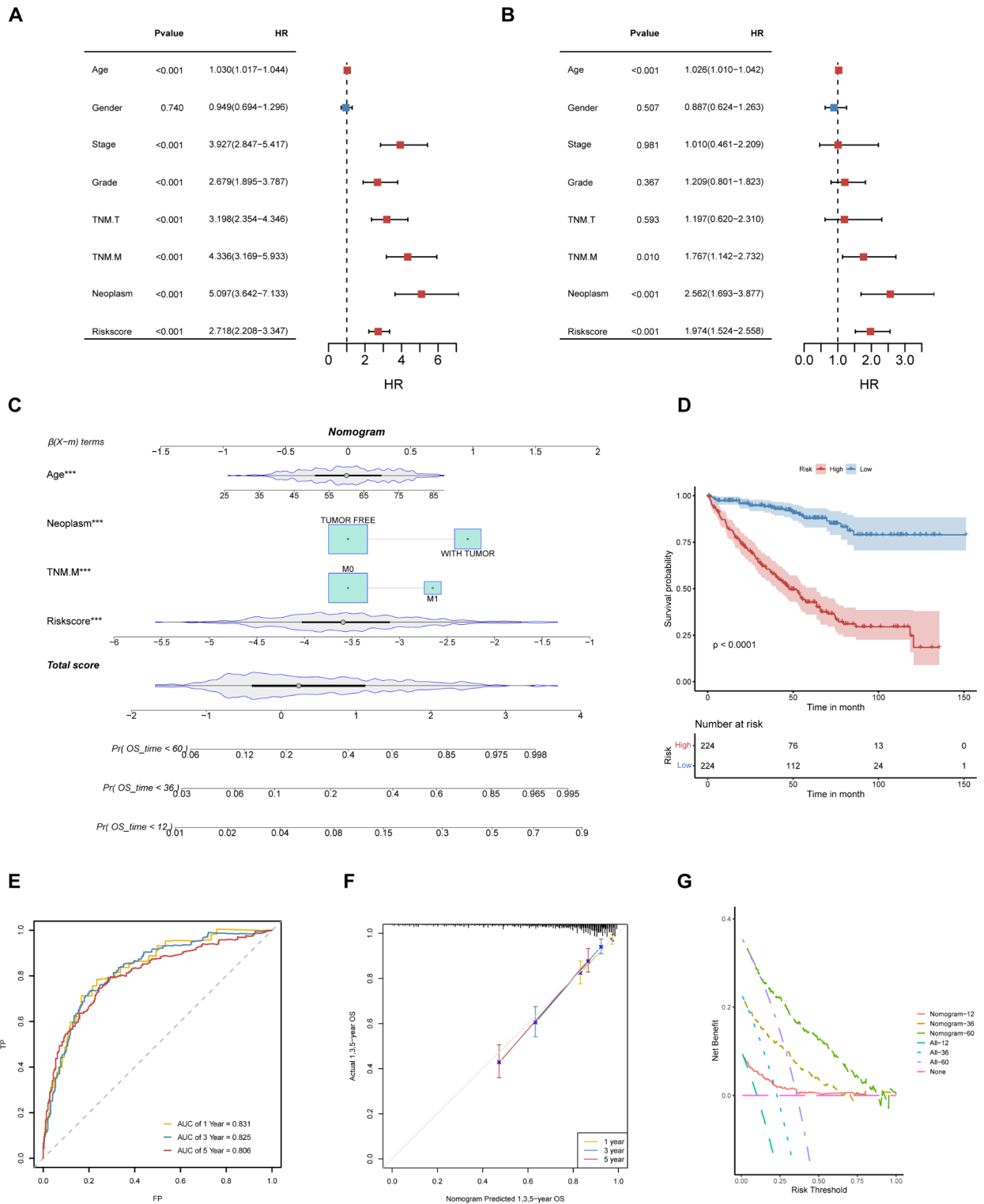
Fig. 7. Establishment and assessment of the nomogram survival model. (**A**). Univariate analysis for the clinicopathologic properties and risk score in TCGA-KIRC. (**B**) Multivariate analysis for the clinicopathologic properties and risk score in TCGA-KIRC. (**C**) A nomogram for predicting the prognosis of KIRC patients. (**D**) Kaplan-Meier analysis for two KIRC groups according to the nomogram score. (**E**) ROC curve analysis of the nomogram in TCGA-KIRC. (**F**) Calibration plots showing the probability of 1-, 3-, and 5-year OS in TCGA-KIRC. (**G**) Decision curve analysis (DCA) of the nomogram predicting 1-, 3-, and 5-year OS.

score was more frequently noted in patients with higher risk scores (Fig. 8A). immune checkpoint inhibitors are anti-tumor immunotherapies. They are being increasingly used in clinical practice. The expression difference of ICGs between the HR and LR groups may result in varying susceptibilities to immune checkpoint inhibitors. According to Fig. 8B the expression level of ICGs differs between the LR group and HR group significantly. The results of immune infiltration analysis revealed that levels of 28 types of immune cells increased significantly in HR patients (Fig. 8C). In particular, there was a significant decrease in the immune infiltration level of resting mast cells, M2 macrophages, monocytes, resting NK cells, and CD8 T cells in HR patients, while that of plasma cells, CD4 memory T cell, and M1 macrophages increased (Fig. 8D). Moreover, 8 genes within the prognostic model were highly correlated with tumor-infiltrating immune cells (Figure S2). Taken together, the results show that ICI may be associated with the ARPS. Additionally, LR patients showed a significantly lower TIDE score compared to HR patients, indicating a better efficacy of immunotherapy (Fig. 8E).

Although the majority of KIRC patients respond very well to platinum-based therapy initially, tumors eventually become increasingly resistant to treatment. Cancer stem cells are extremely rare tumor cells with unique biological properties, such as the capacity of indefinite proliferation, self-renewal, and multiple-direction differentiation to form diverse cell populations within the tumor. As shown in Figure S3, a significantly higher enrichment score of stemness is observed in the HR group by 26 stemness gene sets. Moreover, HR patients had a higher hypoxia score (Fig. 8F) according to the hypoxia-responsive gene expression analysis, and the HR group also had a significantly higher fraction genome altered (Fig. 9A); the CNV analysis revealed that CNV patterns differed significantly between the LR and HR groups (Fig. 9B). As shown in Fig. 9C, when only 20 genes with maximum mutation frequency were contained in the waterfall plot, the distribution of somatic variation in each sample was different between the HR and LR groups. It is interesting to note that an opposite frequency was discovered for BAP1 (HR/LR, 17%/5%) and PBRM1 (HR/LR, 35%/47%) (Fig. 9D).

Drug sensitivity in LR and HR KIRC

Regarding the sensitivity prediction for a number of common drugs, a drug analysis was performed for the LR and HR KIRC. The landscape of the correlation and significance between drug sensitivity and model genes are shown in Fig. 10A. Sunitini (Fig. 10B) and rapamycin (Fig. 10D) exhibited higher sensitivity in the HR KIRC ($p < 0.05$, Wilcoxon rank-sum test). Moreover, Sorafenib (Fig. 10C), imatinib (Fig. 10E), erlotinib (Fig. 10F) and bleomycin (Fig. 10G) exhibited higher sensitivity in the LR KIRC ($p < 0.05$, Wilcoxon rank-sum test).

Identification of biological roles of arPS

Since ARPS had a high prognostic predictive value for KIRC patients, the biological properties were further investigated. The volcano plot visually represents 149 DEGs (Fig. 11A). The string database was applied for creating a PPI network of DEGs (Fig. 11B). GSEA analysis demonstrated that the LR group exhibited a significant enrichment of drug metabolism pathways-CYP450, fatty acid metabolism, fatty acid degradation, and RCC, while the HR group exhibited a significant enrichment of oxidative phosphorylation, p53 signaling pathway, and primary immunodeficiency (Fig. 11C-D). The results of GO analysis demonstrated that the above genes were closely involved in BP of organic anion transport, response to xenobiotic stimulus, renal system process, small molecule catabolic process, carboxylic acid transport, organic acid transport, and cellular response to xenobiotic stimulus (Fig. 11E-F).

Experimental validation for the expression of the key genes

To confirm the signature genes' expression levels, this study examined the expression of SLC28A1, ABCB1, ALDH5A1, ALDH6A1, UGT8, and GSTM3 in human kidney cells. As shown in Fig. 12A, SLC28A1 mRNA in KIRC cell lines (Caki-1, 786-O) was significantly upregulated compared to the normal renal cell line (HK2), while ABCB1, ALDH5A1, ALDH6A1, UGT8, and GSTM3 levels were notably reduced in KIRC cell lines. Additionally, WB experiment also confirmed that in contrast with HK2 cell line, the expression of proteins ABCB1 and ALDH5A1 was downregulated considerably in KIRC cell lines (Fig. 12B). These two experiments also validated the results of the bioinformatics analysis.

Discussion

KIRC, the major pathologic subtype of RCC, represents a substantial global health threat due to its increasing prevalence and high mortality[33]. Although therapeutic strategies for KIRC have progressed significantly, the prognosis for patients with KIRC remains unfavorable, mainly because of resistance to conventional therapies and late diagnosis[34]. Several molecular markers for building predictive models in various cancers have been reported in recent studies. The integration of molecular biomarkers into prognosis models may offer a more comprehensive evaluation of the disease, improve the accuracy of predicting patient outcomes, and ultimately lead to better patient care and outcomes in the management of KIRC.

This study confirmed the critical role of ARGs in KIRC microenvironment, and then created a novel prognosis model on the basis of eight ARGs: ABCB1, ABCG1, ALDH5A1, ALDH6A1, DPEP1, GSTM3, SLC28A1, and UGT8. By spatial transcriptome analysis, we found that ADME related activities were mainly enriched in tumor cells. Besides tumor cells, the scRNA-seq analysis results demonstrated that the ADME related activities also notably enriched in endothelial cell and monocyte/macrophage. Besides tumor cells, tumor microenvironment includes various types of cells, such as tumor immune infiltrating cells and stromal cell. Among these cells, T cell, monocyte, M2-macrophage, endothelial cell and cancer-associated fibroblast are the primary effector tumor immune infiltrating cells and stromal immune cells in cancer immunity, which have close relationships with the start and development of tumor[35]. Among those target genes, ABCB1 gene encodes a permeability glycoprotein. The glycoprotein has expression in the apical membranes of a variety of tissues, including kidney, intestine, liver, blood-brain barrier, placenta, and testis, and is involved in the intracellular drug disposition[36].
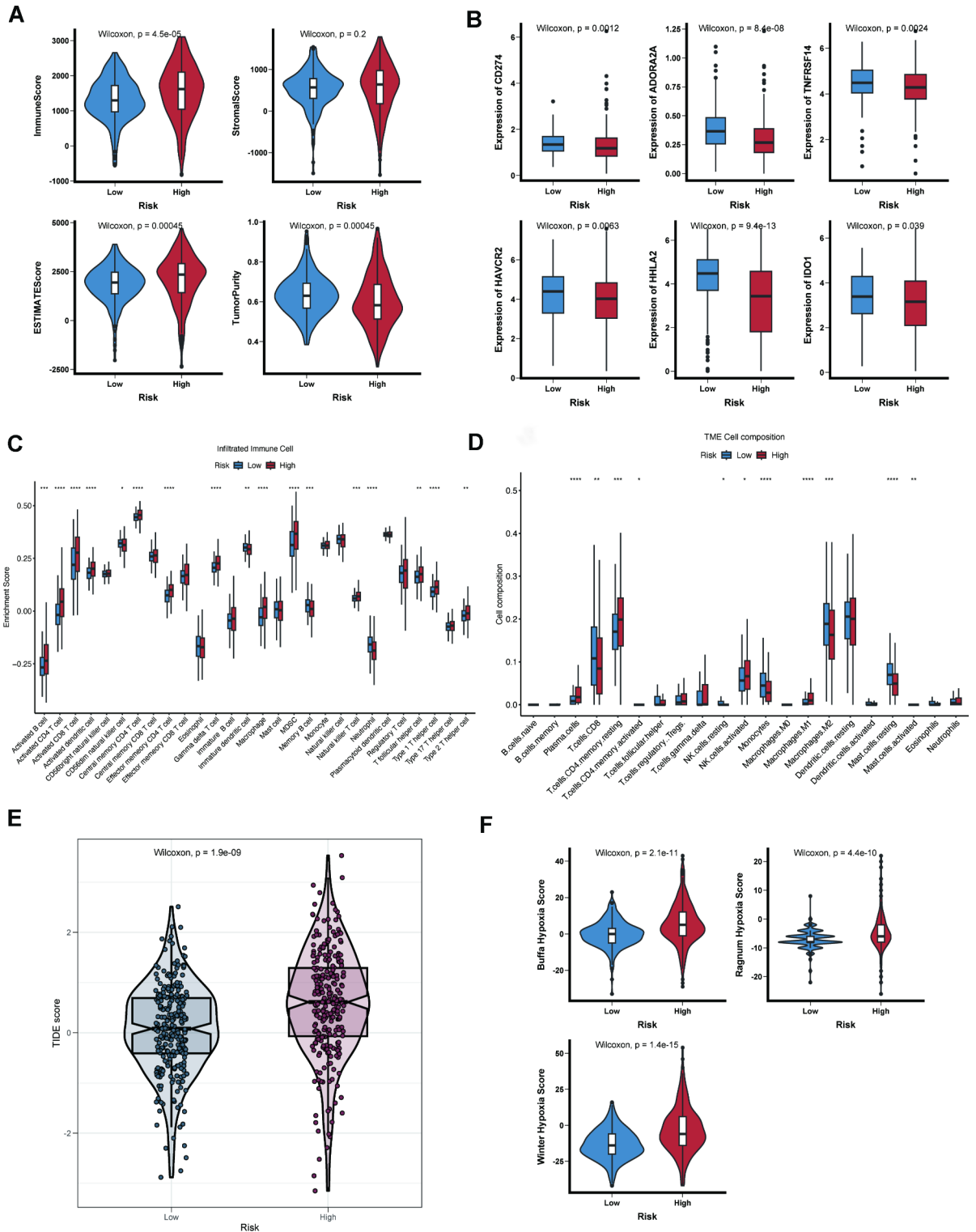
Fig. 8. Immune characteristics of ADME-related prognostic subgroups. (**A**). Violin plot showing lower immune infiltration, stromal, and ESTIMATE scores, and higher tumor purity in HR patients. (**B**) Box plot of expression levels of immune checkpoint- associated genes. (**C**) Box plot of 28 infiltrating immune cell types was calculated by ssGSEA. (**D**) Box plot of 22 infiltrating immune cell types was calculated by CIBERSORT. (**E**) Proportion of response to immunotherapy in the HR and LR groups based on TIDE results. (**F**) Violin plot of significantly increased hypoxic score in HR patients $*p < 0.05$; $**p < 0.01$; $***p < 0.001$; $****p < 0.0001$.
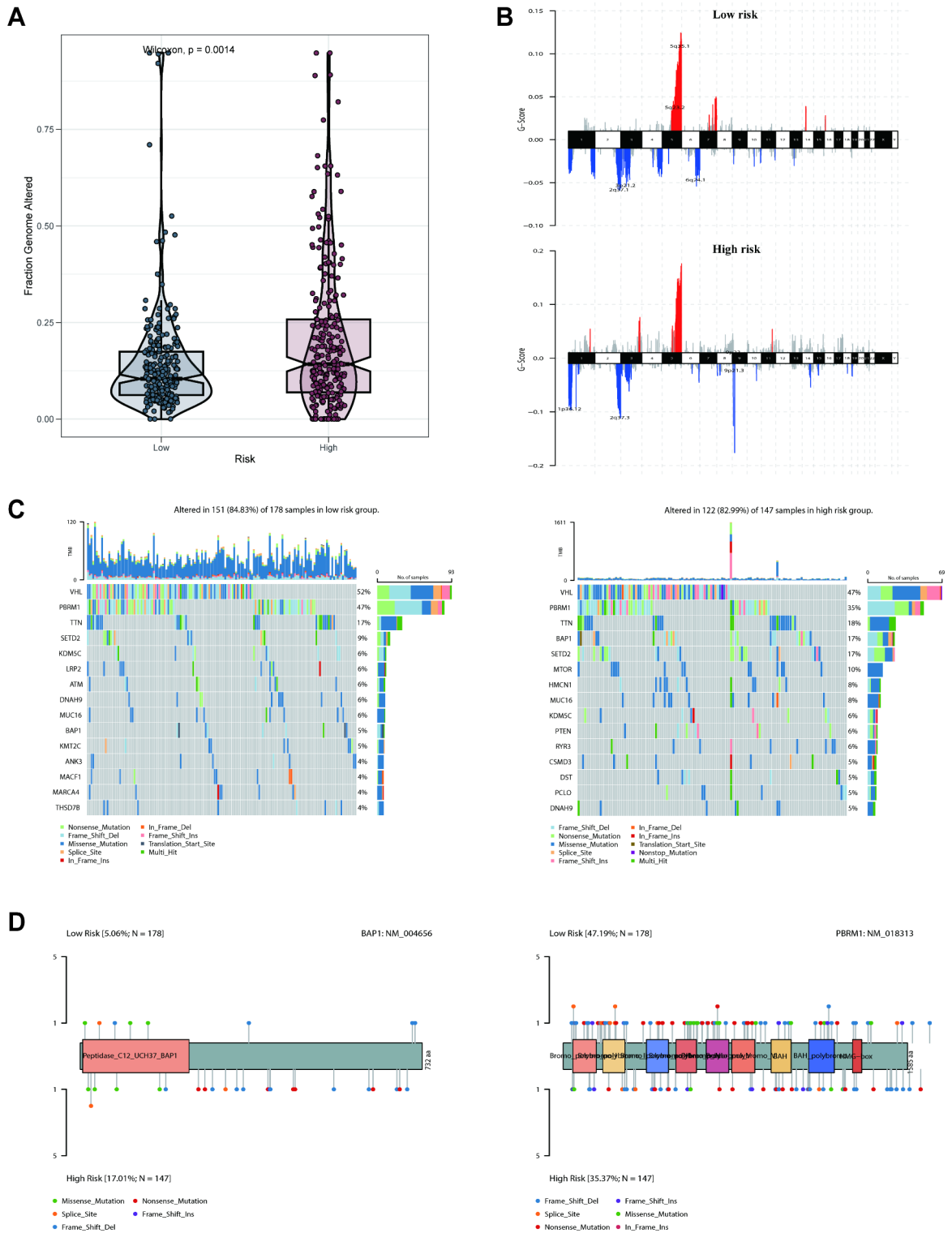
Fig. 9. Mutation landscape between ADME-related prognostic subgroups. (**A**). Difference analysis of fraction genome altered in different risk score groups. (**B**) Patterns of copy number variation (CNV) in different risk cohorts. (**C**) Waterfall plot of somatic mutation characteristics in the HR and LR score groups. (**D**) Comparison of different mutation sites of BAP1 and PBRM1. *$p < 0.05$; ***$p < 0.001$; ****$p < 0.0001$.

Many studies have shown that the ABCB1 overexpression had an association with chemoresistance, reduced survival rates, and poor outcome in patients[36]. The ABC transporter family member ABCG1 is important in tumor immunity, which is found as an oncogene in lung cancer, affecting cell proliferation, migration, invasion, and apoptosis[37]. A study also shows that ABCG1 is linked to KIRC patients' survival, highlighting the potential
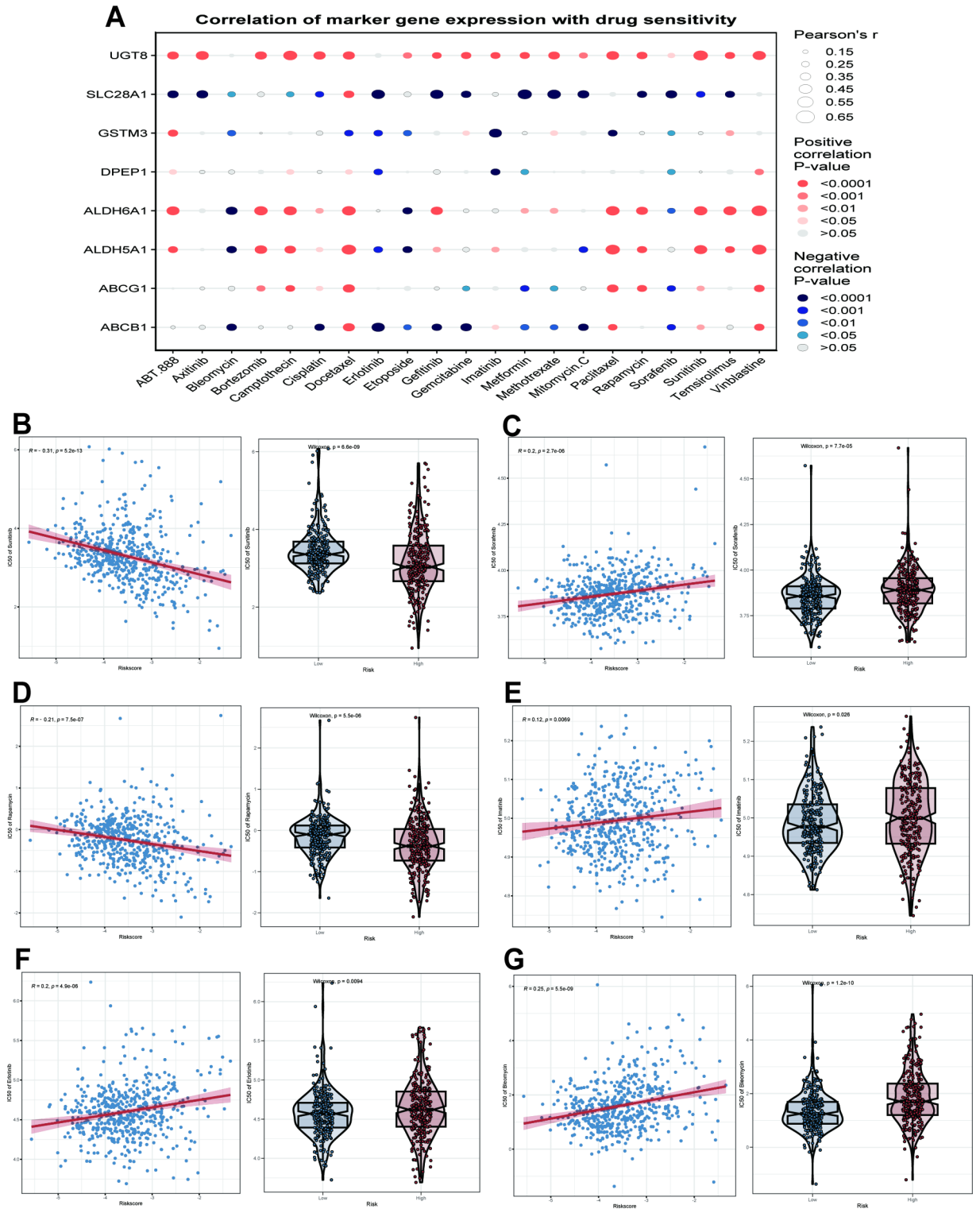
Fig. 10. Effectiveness of ADME-related signature in predicting drug sensitivity. (**A**). Bubble plot of the relationship between drugs and model genes. Boxplots of the comparison of IC50 of drugs between high- and low-risk groups, and correlation between the IC50 and risk score in TCGA-KIRC cohort: (**B**) Sunitinib; (**C**) Sorafenib; (**D**) Rapamycin; (**E**) Imatinib; (**F**) Erlotinib; (**G**) Bleomycin.

value of this gene in cancer diagnosis and prognosis[38]. ALDH5A1, which belongs to the aldehyde dehydrogenase superfamily and encodes succinic semialdehyde dehydrogenase involved in mitochondrial glutamate metabolism, plays critical roles in cell proliferation, differentiation, and survival, with its activation observed in various cancers[39]. It has been demonstrated that the invasion, migration, and proliferation of papillary thyroid
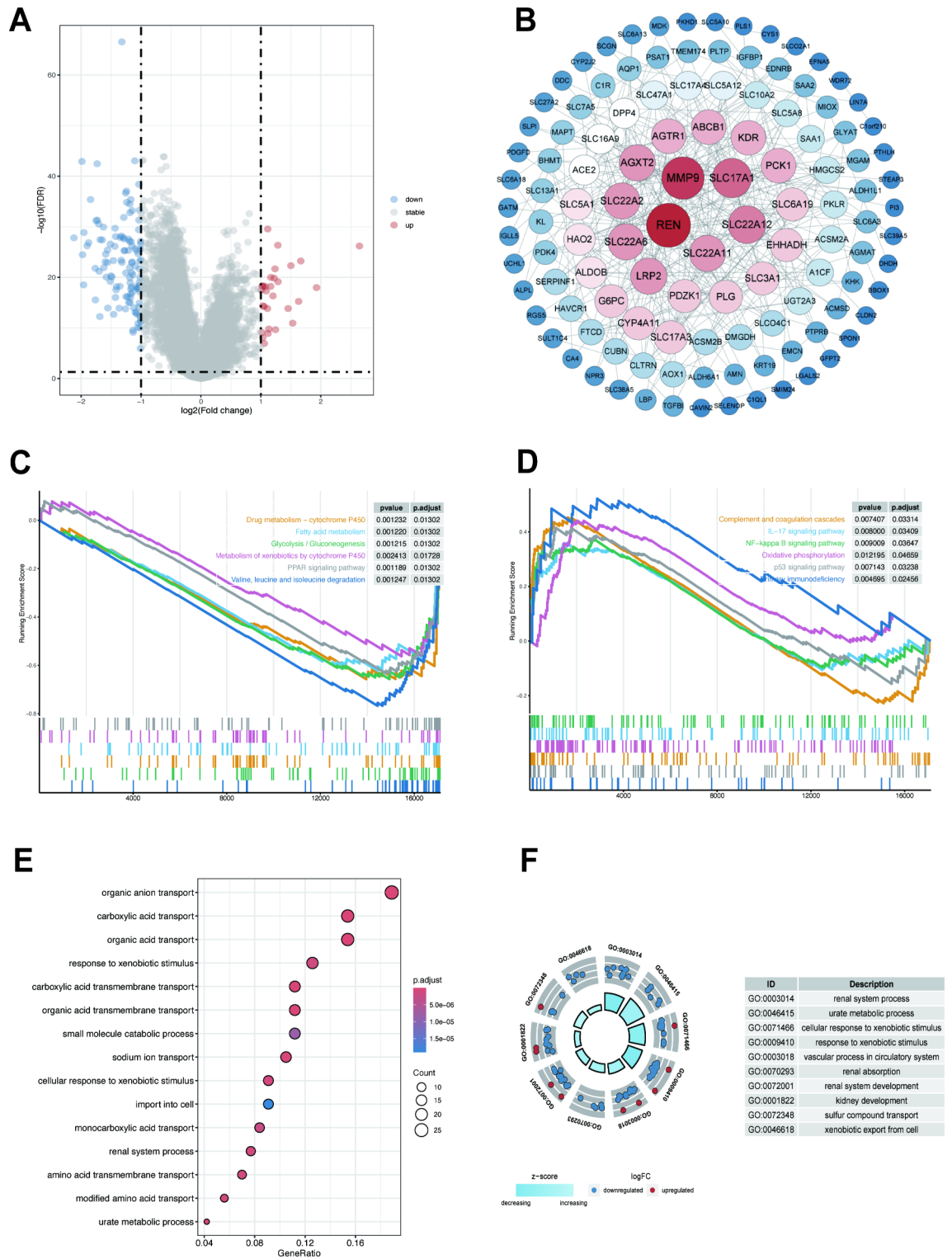
Fig. 11. Biological functions underlying the ADME-related prognosis model. (**A**). Volcano plot for DEGs (FDR < 0.05 and |log2FC| > 0.5) between the HR and LR groups. (**B**) PPI network of Risk-related DEGs. GSEA analysis of KEGG pathways between (**C**) LR group; (**D**) HR group. (**E**) Dot plot of GO BP enrichment analysis. (**F**) GO circle plot of enriched GO BP terms.

carcinoma (PTC) cells may be inhibited by ALDH5A1 knockdown[40]. Similarly, the decreased expression of ALDH5A1 has been correlated with a positive prognosis in ovarian cancer[39]. ALDH6A1 is another member of the aldehyde dehydrogenase superfamily and has been shown to have a role in cancer[41]. Based on the analysis of the TCGA database, ALDH6A1 shows differential expression in KIRC compared to normal individuals.
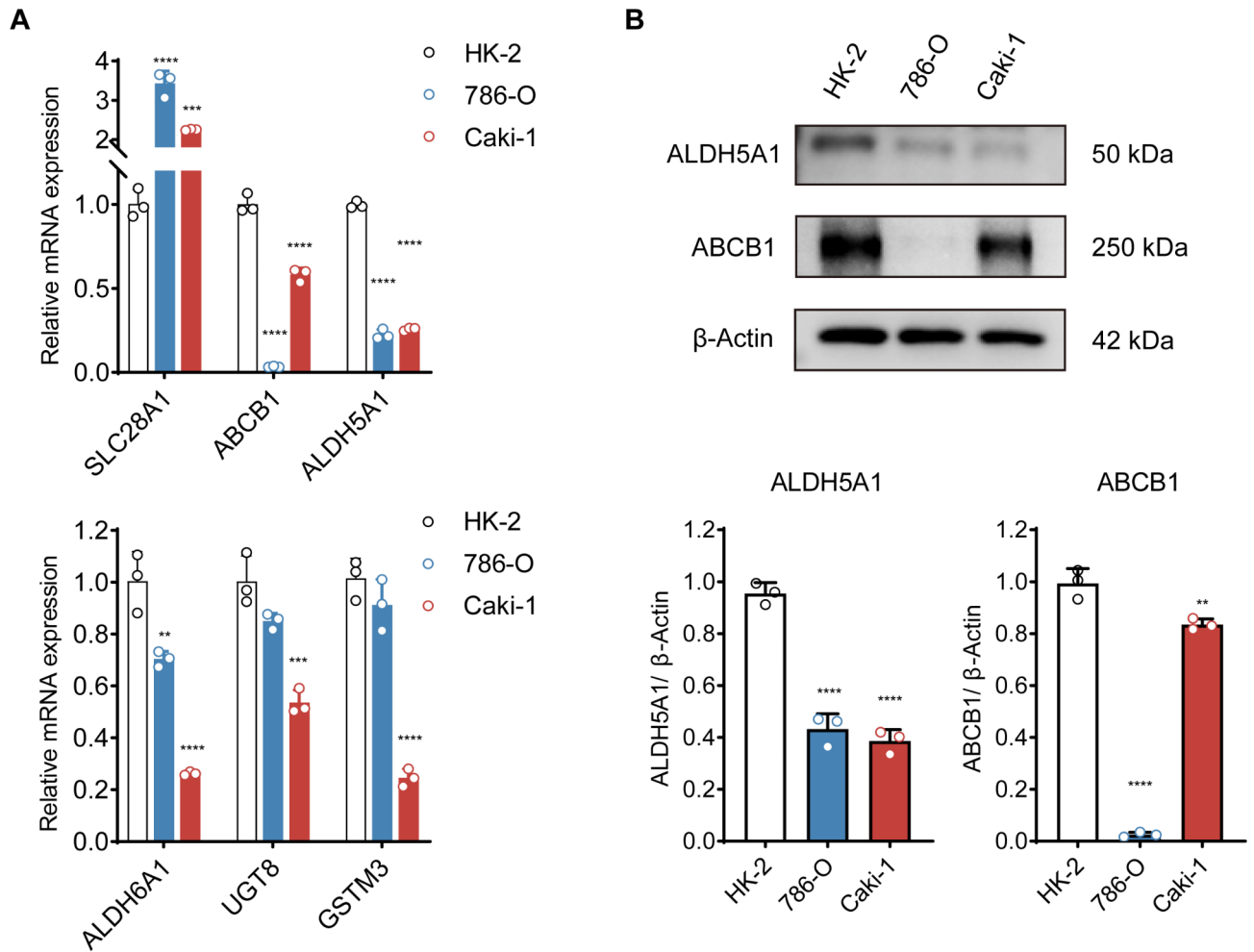
Fig. 12. Validation of ADME-related signature genes expression. (**A**) The mRNA levels of SLC28A1, ABCB1, ALDH5A1, ALDH6A1, UGT8, and GSTM3 were examined by qRT-PCR. (**B**) The protein levels of ABCB1 and ALDH5A1 were examined by WB. $**p < 0.01$; $***p < 0.001$, $****p < 0.0001$.

Moreover, overexpression of ALDH6A1 can inhibit renal cancer cells from growing and migrating[42]. DPEP1, a zinc-dependent metalloproteinase that plays a role in glutathione metabolism via dipeptide hydrolysis, has recently been implicated in human malignancies[43]. In particular, its dysregulation is common in several cancers, including hepatoblastoma, pancreatic ductal adenocarcinoma and KIRC. GSTM3, one of glutathione S-transferase Mu gene family members, plays a crucial role in detoxifying electrophilic compounds, including products of oxidative stress, anticarcinogens, and carcinogenic toxins, by conjugating with glutathione[44]. In ovarian cancer, GSTM3 expression has been correlated with immune evasion, chemoresistance, and poor prognosis[45]. In ESCC, a high GSTM3 expression is negatively linked to DFS[46]. Moreover, GSTM3 plays a pivotal role in KIRC by detoxifying and scavenging ROS[47]. SLC28A1, also referred to as concentrating nucleoside transporter 1, is a type of nucleoside transporter that is mainly responsible for cellular absorption of nucleosides and related compounds, including gemcitabine and 5-fluorouracil[48]. UGT8 exhibits elevated expression in various cancers, indicating the potential for intratumoral drug metabolism via the UGT conjugation pathway[49]. One study has demonstrated that UGT8 expression significantly increases in KIRC and correlates with decreased overall patient survival[49].

Functional analyses were conducted to examine the biological roles of ARGs in KIRC in line with DEGs between HR and LR groups. GO and KEGG analyses demonstrated that the LR group exhibited an enrichment of pathways associated with metabolism, including fatty acid metabolism, xenobiotic metabolism by CYP450, PPAR signaling pathway, and drug metabolism-CYP450, while the HR group exhibited an enrichment of those related to primary immunodeficiency and NF-kappa B signaling pathway. Unfavorable prognosis of KIRC was linked to CYP450 dysregulation[50]. CYP3A subfamily of CYP450 enzymes plays an important role in clearance and metabolism of numerous anticancer medications. The presence and activity of these enzymes in KIRC tumor cells may affect drug PK and contribute to drug resistance[51]. Additionally, KIRC is characterized by the abnormal accumulation of lipid droplets in cells, a manifestation of dysregulated cellular metabolism[52,53]. Such metabolic dysregulation is central to the onset and advancement of a disease[54]. Studies have shown metabolic reprogramming in KIRC, including changes in lipid metabolism, some of which may be mediated

by PPAR pathway dysregulation[55]. In contrast, HR KIRC patients exhibit features associated with primary immunodeficiency, such as decreased antigen presentation and T-cell co-stimulation, along with increased expression of immune checkpoint molecules including PDCD1 and CTLA4[56]. These findings suggest an immunosuppressive TME in the HR KIRC group, which may contribute to their poorer prognosis. The NF-κB signaling pathway was discovered to be considerably enriched in HR KIRC patients and appeared to have a key role in the onset, advancement, and immune evasion of KIRC[57].

A powerful tool for risk stratification of patients is the in-depth molecular characterization of tumor heterogeneity. The results of this study showed that HR patients have a higher level of CNV mutation, TIDE score or hypoxia score compared to LR patients. The results revealed that patients in HR group did not respond well to immunotherapy. Furthermore, mutations in tumor suppressor genes were more frequent in the HR group (such as BAP1 and SETD2). BAP1 mutations can also lead to a "cold" TME[58]. Patients with BAP1 mutations may be less responsive to immunotherapy because the "cold" TME created by these mutations may confer resistance[58]. SETD2 mutations are linked to an inflamed and immunogenic TME, which may contribute to an improved response to immunotherapy in KIRC[59].

Additionally, the results demonstrated that the LR and HR groups differ significantly in the characteristics of ICI. HR patients had a significantly reduced immune infiltration level of M2 macrophages, resting NK cells, and CD8 T cells and an elevated level of CD4 memory T cells. The disease progression and patient prognosis were influenced by important factors such as the composition and dynamics of ICI in TME of KIRC, particularly the levels of CD8$^+$ T cells[60]. A higher CD8$^+$ T cell infiltration level in KIRC is generally correlated with a reduced possibility of metastatic disease and a better prognosis[61]. Conversely, patients with KIRC who develop metastatic disease typically have increased levels of exhausted or dysfunctional CD8$^+$ T cells in TME[61]. Similar to the results in this study, studies reveal that a higher proportion of NK cells in tumor-infiltrating lymphocytes is correlated with a better prognosis in RCC[62]. Qin et al. found that the KIRC subtype B, which had the highest infiltration of M2 macrophages, had a better OS compared with the other KIRC subtypes, suggesting that a higher M2 macrophage infiltration is correlated with a better prognosis in KIRC[63]. However, the complexity of TME in RCC tumors still exists. For example, Chen et al. found that a long OS was predicted by a high level of tumor-infiltrating dendritic cells and CD4$^+$ T cells in KIRC, whereas macrophages, monocytes, MDSCs, Tfhs, Tregs, and NK cells suggested shorter OS[64].

Limitations

ARGs are promising as innovative diagnostic and therapeutic markers for KIRC. However, this study has several potential limitations. First, it does not describe the underlying biological mechanisms or interactions. In addition, the results, derived retrospectively from public databases, need to be further validated by extensive prospective studies before their clinical application. Finally, the statistical validity of the study's findings may be jeopardized by the lack of comprehensive treatment data.

Conclusion

In summary, this study represents the first effort to confirm the key role of ARGs in KIRC microenvironment using scRNA-seq analysis and spatial transcriptome analysis, and then develop a prognosis model for KIRC based on ARGs, and then constructed a novel ARPS of KIRC using a TCGA cohort, which is validated in an external cohort, and qRT-PCR and western blot experiment. This risk model showed a good performance in predicting patient survival. In addition, it was found that there was an association between the ARS and ICI in KIRC. This study offers a promising ARPS to guide the personalized treatment for KIRC patients. Furthermore, it provides a new insight into possible immunotherapeutic and combined strategies for KIRC, as targeting ARGs may reverse ICI in KIRC.

Data availability

All the datasets presented in this study can be found in the article. Further inquiries can be directed to Dr. Jun Yuan at yjun_92@hbucm.edu.cn.

References
1. Siegel, R. L., Miller, K. D. & Jemal, A. Cancer statistics, 2018. *CA Cancer J Clin* **68**, 7–30. https://doi.org/10.3322/caac.21442 (2018).
2. Hsieh, J. J. et al. Renal cell carcinoma. *Nat Rev Dis Primers* **3**, 17009. https://doi.org/10.1038/nrdp.2017.9 (2017).
3. Li, Q. K., Pavlovich, C. P., Zhang, H., Kinsinger, C. R. & Chan, D. W. Challenges and opportunities in the proteomic characterization of clear cell renal cell carcinoma (ccRCC): A critical step towards the personalized care of renal cancers. *Semin Cancer Biol* **55**, 8–15. https://doi.org/10.1016/j.semcancer.2018.06.004 (2019).
4. Makino, T., Kadomoto, S., Izumi, K. & Mizokami, A. Epidemiology and prevention of renal cell carcinoma. *Cancers* https://doi.org/10.3390/cancers14164059 (2022).
5. Cui, Y. Q., Meng, F., Zhan, W. L., Dai, Z. T. & Liao, X. High expression of GSDMC is associated with poor survival in kidney clear cell cancer. *Biomed Res Int* **2021**, 5282894. https://doi.org/10.1155/2021/5282894 (2021).
6. Padala, S. A. et al. Epidemiology of renal cell carcinoma. *World J Oncol* **11**, 79–87. https://doi.org/10.14740/wjon1279 (2020).
7. Hu, D. G., Marri, S., McKinnon, R. A., Mackenzie, P. I. & Meech, R. Deregulation of the genes that are involved in drug absorption, distribution, metabolism, and excretion in hepatocellular carcinoma. *J Pharmacol Exp Ther* **368**, 363–381. https://doi.org/10.1124/jpet.118.255018 (2019).
8. Hovelson, D. H. et al. Characterization of ADME gene variation in 21 populations by exome sequencing. *Pharmacogenet Genomics* **27**, 89–100. https://doi.org/10.1097/fpc.0000000000000260 (2017).
9. Wang, J. *et al.* Identification and validation of ADME genes as prognosis and therapy markers for hepatocellular carcinoma patients. *Biosci Rep* **41**. 10.1042/bsr20210583 (2021).

10. Hu, D. G., Mackenzie, P. I., Nair, P. C., McKinnon, R. A. & Meech, R. The expression profiles of ADME genes in human cancers and their associations with clinical outcomes. *Cancers* https://doi.org/10.3390/cancers12113369 (2020).

11. Tang, X. et al. Development and validation of an ADME-related gene signature for survival, treatment outcome and immune cell infiltration in head and neck squamous cell carcinoma. *Front Immunol* **13**, 905635. https://doi.org/10.3389/fimmu.2022.905635 (2022).

12. Rehman, K. et al. Analysis of genetic biomarkers, polymorphisms in ADME-related genes and their impact on pharmacotherapy for prostate cancer. *Cancer Cell Int* **23**, 247. https://doi.org/10.1186/s12935-023-03084-5 (2023).

13. Wang, J., Wang, G., Hu, T., Wang, H. & Zhou, Y. Identification of an ADME-related gene for forecasting the prognosis and responding to immunotherapy in sarcomas. *Eur J Med Res* **29**, 45. https://doi.org/10.1186/s40001-023-01624-3 (2024).

14. Tomczak, K., Czerwińska, P. & Wiznerowicz, M. The Cancer Genome Atlas (TCGA): an immeasurable source of knowledge. *Contemp Oncol (Pozn)* **19**, A68-77. https://doi.org/10.5114/wo.2014.47136 (2015).

15. Colaprico, A. et al. TCGAbiolinks: An R/Bioconductor package for integrative analysis of TCGA data. *Nucleic Acids Res* **44**, e71. https://doi.org/10.1093/nar/gkv1507 (2016).

16. Sun, Z. et al. Construction of a lactate-related prognostic signature for predicting prognosis, tumor microenvironment, and immune response in kidney renal clear cell carcinoma. *Front Immunol* **13**, 818984. https://doi.org/10.3389/fimmu.2022.818984 (2022).

17. Sun, D. et al. TISCH: A comprehensive web resource enabling interactive single-cell transcriptome visualization of tumor microenvironment. *Nucleic Acids Res* **49**, D1420-d1430. https://doi.org/10.1093/nar/gkaa1020 (2021).

18. Slovin, S. et al. Single-cell RNA sequencing analysis: A step-by-step overview. *Methods Mol Biol* **2284**, 343–365. https://doi.org/10.1007/978-1-0716-1307-8_19 (2021).

19. Hafemeister, C. & Satija, R. Normalization and variance stabilization of single-cell RNA-seq data using regularized negative binomial regression. *Genome Biol* **20**, 296. https://doi.org/10.1186/s13059-019-1874-1 (2019).

20. Lin, W. et al. The activity of cuproptosis pathway calculated by AUCell algorithm was employed to construct cuproptosis landscape in lung adenocarcinoma. *Discov Oncol* **14**, 135. https://doi.org/10.1007/s12672-023-00755-7 (2023).

21. Hu, C. et al. Cell Marker 2.0: An updated database of manually curated cell markers in human/mouse and web tools based on scRNA-seq data. *Nucleic Acids Res* **51**, D870–D876. https://doi.org/10.1093/nar/gkac947 (2023).

22. Ritchie, M. E. et al. limma powers differential expression analyses for RNA-sequencing and microarray studies. *Nucleic Acids Res* **43**, e47. https://doi.org/10.1093/nar/gkv007 (2015).

23. Kanehisa, M. & Goto, S. KEGG: Kyoto encyclopedia of genes and genomes. *Nucleic Acids Res* **28**, 27–30. https://doi.org/10.1093/nar/28.1.27 (2000).

24. Kanehisa, M., Furumichi, M., Sato, Y., Kawashima, M. & Ishiguro-Watanabe, M. KEGG for taxonomy-based analysis of pathways and genomes. *Nucleic Acids Res* **51**, D587-d592. https://doi.org/10.1093/nar/gkac963 (2023).

25. Kanehisa, M. Toward understanding the origin and evolution of cellular organisms. *Protein Sci* **28**, 1947–1951. https://doi.org/10.1002/pro.3715 (2019).

26. Yu, G., Wang, L. G., Han, Y. & He, Q. Y. clusterProfiler: An R package for comparing biological themes among gene clusters. *Omics* **16**, 284–287. https://doi.org/10.1089/omi.2011.0118 (2012).

27. Chen, C. et al. Tumor immune cell infiltration score based model predicts prognosis in multiple myeloma. *Sci Rep* **12**, 17082. https://doi.org/10.1038/s41598-022-21763-7 (2022).

28. Chen, B., Khodadoust, M. S., Liu, C. L., Newman, A. M. & Alizadeh, A. A. Profiling tumor infiltrating immune cells with CIBERSORT. *Methods Mol Biol* **1711**, 243–259. https://doi.org/10.1007/978-1-4939-7493-1_12 (2018).

29. Zheng, K. et al. Tumor immune dysfunction and exclusion subtypes in bladder cancer and pan-cancer: A novel molecular subtyping strategy and immunotherapeutic prediction model. *J Transl Med* **22**, 365. https://doi.org/10.1186/s12967-024-05186-8 (2024).

30. Gao, J. et al. Integrative analysis of complex cancer genomics and clinical profiles using the cBioPortal. *Sci Signal* **6**, 11. https://doi.org/10.1126/scisignal.2004088 (2013).

31. Geeleher, P., Cox, N. & Huang, R. S. pRRophetic: An R package for prediction of clinical chemotherapeutic response from tumor gene expression levels. *PLoS ONE* **9**, e107468. https://doi.org/10.1371/journal.pone.0107468 (2014).

32. Pinto, J. P. et al. StemChecker: A web-based tool to discover and explore stemness signatures in gene sets. *Nucleic Acids Res* **43**, W72-77. https://doi.org/10.1093/nar/gkv529 (2015).

33. Xia, D., Liu, Q., Yan, S. & Bi, L. Construction of a prognostic model for KIRC and identification of drugs sensitive to therapies: A comprehensive biological analysis based on m6A-related LncRNAs. *Front Oncol* **12**, 895315. https://doi.org/10.3389/fonc.2022.895315 (2022).

34. Liao, G., Wang, P. & Wang, Y. Identification of the prognosis value and potential mechanism of immune checkpoints in renal clear cell carcinoma microenvironment. *Front Oncol* **11**, 720125. https://doi.org/10.3389/fonc.2021.720125 (2021).

35. Arneth, B. Tumor Microenvironment. *Medicina* https://doi.org/10.3390/medicina56010015 (2019).

36. Abd El-Aziz, Y. S., Spillane, A. J., Jansson, P. J. & Sahni, S. Role of ABCB1 in mediating chemoresistance of triple-negative breast cancers. *Biosci Rep* **41**. 10.1042/bsr20204092 (2021).

37. Tian, C. et al. ABCG1 as a potential oncogene in lung cancer. *Exp Ther Med* **13**, 3189–3194. https://doi.org/10.3892/etm.2017.4393 (2017).

38. Meng, F., Xiao, Y., Xie, L., Liu, Q. & Qian, K. Diagnostic and prognostic value of ABC transporter family member ABCG1 gene in clear cell renal cell carcinoma. *Channels* **15**, 375–385. https://doi.org/10.1080/19336950.2021.1909301 (2021).

39. Tian, X. et al. Decreased expression of ALDH5A1 predicts prognosis in patients with ovarian cancer. *Cancer Biol Ther* **18**, 245–251. https://doi.org/10.1080/15384047.2017.1295175 (2017).

40. Deng, X. Y. et al. ALDH5A1 acts as a tumour promoter and has a prognostic impact in papillary thyroid carcinoma. *Cell Biochem Funct* **39**, 317–325. https://doi.org/10.1002/cbf.3584 (2021).

41. Cai, Y. et al. The downregulated drug-metabolism related ALDH6A1 serves as predictor for prognosis and therapeutic immune response in gastric cancer. *Aging* **14**, 7038–7051. https://doi.org/10.18632/aging.204270 (2022).

42. Lu, J. et al. ABAT and ALDH6A1, regulated by transcription factor HNF4A, suppress tumorigenic capability in clear cell renal cell carcinoma. *J Transl Med* **18**, 101. https://doi.org/10.1186/s12967-020-02268-1 (2020).

43. Cui, X. et al. DPEP1 is a direct target of miR-193a-5p and promotes hepatoblastoma progression by PI3K/Akt/mTOR pathway. *Cell Death Dis* **10**, 701. https://doi.org/10.1038/s41419-019-1943-0 (2019).

44. Nebert, D. W. & Vasiliou, V. Analysis of the glutathione S-transferase (GST) gene family. *Hum Genomics* **1**, 460–464. https://doi.org/10.1186/1479-7364-1-6-460 (2004).

45. Zhang, J. et al. Comprehensive analysis of the glutathione S-transferase Mu (GSTM) gene family in ovarian cancer identifies prognostic and expression significance. *Front Oncol* **12**, 968547. https://doi.org/10.3389/fonc.2022.968547 (2022).

46. Jain, M. et al. Role of GSTM3 polymorphism in the risk of developing esophageal cancer. *Cancer Epidemiol Biomarkers Prev* **16**, 178–181. https://doi.org/10.1158/1055-9965.Epi-06-0542 (2007).

47. Wang, Y. et al. A novel functional polymorphism of GSTM3 reduces clear cell renal cell carcinoma risk through enhancing its expression by interfering miR-556 binding. *J Cell Mol Med* **22**, 3005–3015. https://doi.org/10.1111/jcmm.13528 (2018).

48. Scionti, F. et al. Risk alleles for multiple myeloma susceptibility in ADME genes. *Cells* https://doi.org/10.3390/cells11020189 (2022).

49. Hu, D. G. et al. The expression profiles and deregulation of UDP-glycosyltransferase (UGT) genes in human cancers and their association with clinical outcomes. *Cancers* https://doi.org/10.3390/cancers13174491 (2021).

50. Guo, X., Sun, Z., Jiang, S., Jin, X. & Wang, H. Identification and validation of a two-gene metabolic signature for survival prediction in patients with kidney renal clear cell carcinoma. *Aging* **13**, 8276–8289. https://doi.org/10.18632/aging.202636 (2021).

51. McFadyen, M. C., Melvin, W. T. & Murray, G. I. Cytochrome P450 CYP1B1 activity in renal cell carcinoma. *Br J Cancer* **91**, 966–971. https://doi.org/10.1038/sj.bjc.6602053 (2004).

52. Liu, M. et al. A cluster of metabolism-related genes predict prognosis and progression of clear cell renal cell carcinoma. *Sci Rep* **10**, 12949. https://doi.org/10.1038/s41598-020-67760-6 (2020).

53. Li, H. & Mo, Z. Prognostic value of metabolism-related genes and immune infiltration in clear cell renal cell carcinoma. *Int J Gen Med* **14**, 6885–6898. https://doi.org/10.2147/ijgm.S328109 (2021).

54. Zhang, J. et al. Metabolism-related signature analysis uncovers the prognostic and immunotherapeutic characteristics of renal cell carcinoma. *Front Mol Biosci* **9**, 837145. https://doi.org/10.3389/fmolb.2022.837145 (2022).

55. di Meo, N. A. et al. Renal cell carcinoma as a metabolic disease: An update on main pathways, potential biomarkers, and therapeutic targets. *Int J Mol Sci* **23**, 66. https://doi.org/10.3390/ijms232214360 (2022).

56. Weng, Y. & Ning, P. Construction of a prognostic prediction model for renal clear cell carcinoma combining clinical traits. *Sci Rep* **13**, 3358. https://doi.org/10.1038/s41598-023-30020-4 (2023).

57. Sun, J., Chen, F. & Wu, G. Role of NF-κB pathway in kidney renal clear cell carcinoma and its potential therapeutic implications. *Aging* **15**, 11313–11330. https://doi.org/10.18632/aging.205129 (2023).

58. Tan, G. et al. The critical role of BAP1 mutation in the prognosis and treatment selection of kidney renal clear cell carcinoma. *Transl Androl Urol* **9**, 1725–1734. https://doi.org/10.21037/tau-20-1079 (2020).

59. Niu, N. et al. Tumor cell-intrinsic SETD2 deficiency reprograms neutrophils to foster immune escape in pancreatic tumorigenesis. *Adv Sci* **10**, e2202937. https://doi.org/10.1002/advs.202202937 (2023).

60. Zheng, Y. et al. Global characterization of immune infiltration in clear cell renal cell carcinoma. *Onco Targets Ther* **14**, 2085–2100. https://doi.org/10.2147/ott.S282763 (2021).

61. Shapiro, D. D. et al. Non-metastatic clear cell renal cell carcinoma immune cell infiltration heterogeneity and prognostic ability in patients following surgery. *Cancers* https://doi.org/10.3390/cancers16030478 (2024).

62. Cózar, J. M. et al. Analysis of NK cells and chemokine receptors in tumor infiltrating CD4 T lymphocytes in human renal carcinomas. *Cancer Immunol Immunother* **54**, 858–866. https://doi.org/10.1007/s00262-004-0646-1 (2005).

63. Qin, H., Wang, T. & Zhang, H. Identification of immune-related subtypes and characterization of tumor microenvironment infiltration in kidney renal clear cell carcinoma. *Front Genet* **13**, 906113. https://doi.org/10.3389/fgene.2022.906113 (2022).

64. Chen, Z., Wu, R., Ma, J. & Zheng, J. C chemokines are prognostic biomarkers correlated with diverse immune cell infiltrations in clear cell renal cell carcinoma. *Transl Cancer Res* **11**, 2501–2522. https://doi.org/10.21037/tcr-22-424 (2022).

Author contributions

Conceptualization: H.W. and F.L.; Methodolog: X.Z.; Data curation: Q.W. and X.G; Formal analysis, H.W.and F.L.; Supervision: X.G. and X.C.; Writing-original draft preparation: H.W. ; Writing-review and editing: J.Y. and X.Z.; All authors have read and approved the published version of the manuscript.

Funding

Declarations

Competing interests

The authors declare no competing interests.

Cell lines identity

The human kidney cell lines, including HK-2, 786-O, and Caki-1, were purchased from Wuhan Pricella Biotechnology Co.

Additional information

Supplementary Information The online version contains supplementary material available at https://doi.org/10.1038/s41598-024-84018-7.

Correspondence and requests for materials should be addressed to X.Z. or J.Y.

Reprints and permissions information is available at www.nature.com/reprints.

Publisher's note Springer Nature remains neutral with regard to jurisdictional claims in published maps and institutional affiliations.